



Coupling global models for hydrology and nutrient loading

A. H. W. Beusen et al.

Coupling global models for hydrology and nutrient loading to simulate nitrogen and phosphorus retention in surface water – description of IMAGE-GNM and analysis of performance

A. H. W. Beusen^{1,2}, L. P. H. Van Beek³, A. F. Bouwman^{1,2}, J. M. Mogollón¹, and J. J. Middelburg¹

¹Department of Earth Sciences – Geochemistry, Faculty of Geosciences, Utrecht University, P.O. Box 80.021, 3508 TA Utrecht, the Netherlands

²PBL Netherlands Environmental Assessment Agency, P.O. Box 303, 3720 AH Bilthoven, the Netherlands

³Department of Physical Geography, Faculty of Geosciences, Utrecht University, P.O. Box 80.115, 3508 TC Utrecht, the Netherlands

Title Page

Abstract

Introduction

Conclusions

References

Tables

Figures



Back

Close

Full Screen / Esc

Printer-friendly Version

Interactive Discussion



Received: 1 June 2015 – Accepted: 17 July 2015 – Published: 3 September 2015

Correspondence to: A. H. W. Beusen (arthur.beusen@pbl.nl)

Published by Copernicus Publications on behalf of the European Geosciences Union.

GMDD

8, 7477–7539, 2015

Coupling global models for hydrology and nutrient loading

A. H. W. Beusen et al.

Title Page

Abstract

Introduction

Conclusions

References

Tables

Figures



Back

Close

Full Screen / Esc

Printer-friendly Version

Interactive Discussion



Abstract

The IMAGE-Global Nutrient Model (GNM) is a global distributed spatially explicit model using hydrology as the basis for describing nitrogen (N) and phosphorus (P) delivery to surface water and transport and in-stream retention in rivers, lakes, wetlands and reservoirs. It is part of the integrated assessment model IMAGE, which studies the interaction between society and the environment over prolonged time periods. In the IMAGE-GNM model, grid cells receive water with dissolved and suspended N and P from upstream grid cells; inside grid cells, N and P are delivered to water bodies via diffuse sources (surface runoff, shallow and deep groundwater, riparian zones; litterfall in floodplains; atmospheric deposition) and point sources (wastewater); N and P retention in a water body is calculated on the basis of the residence time of the water and nutrient uptake velocity; subsequently, water and nutrients are transported to downstream grid cells. Differences between model results and observed concentrations for a range of global rivers are acceptable given the global scale of the uncalibrated model. Sensitivity analysis with data for the year 2000 showed that runoff is a major factor for N and P delivery, retention and river export. For both N and P, uptake velocity and all factors used to compute the subgrid in-stream retention are important for total in-stream retention and river export. Soil N budgets, wastewater and all factors determining litterfall in floodplains are important for N delivery to surface water. For P the factors that determine the P content of the soil (soil P content and bulk density) are important factors for delivery and river export.

1 Introduction

Eutrophication, induced by a surge in anthropogenic nutrient loads to the global freshwater domain (e.g. rivers, lakes, and estuaries), has an increasingly negative impact on aquatic ecosystems. In order to ameliorate and reverse this trend, ecological principles must be integrated into environmental management and restoration practices. These

GMDD

8, 7477–7539, 2015

Coupling global models for hydrology and nutrient loading

A. H. W. Beusen et al.

Title Page

Abstract

Introduction

Conclusions

References

Tables

Figures



Back

Close

Full Screen / Esc

Printer-friendly Version

Interactive Discussion



Coupling global models for hydrology and nutrient loading

A. H. W. Beusen et al.

Title Page

Abstract

Introduction

Conclusions

References

Tables

Figures



Back

Close

Full Screen / Esc

Printer-friendly Version

Interactive Discussion



actions require a thorough understanding of the interactions between various human-induced disturbances (e.g. climate change, land use change, nutrient loadings and hydrology regulation) and their effects on freshwater systems (Stanley et al., 2010). To fully grasp the human impact on biogeochemical cycles, studies must collectively consider the biogeochemical turnover and exchange among the atmosphere, and the aquatic and terrestrial ecosystems.

Numerical models can assess the interaction between multiple processes in various river basin environments. They can furthermore improve predictions for the regional to global nutrient flux from the land to the ocean. Integrated Assessment Models (IAM) have established themselves as powerful tools to study future development of complex, large-scale environmental and sustainable development issues. There are at least two key reasons for this: (i) many of these issues are strongly interlinked and integrated models can capture important consequences of these linkages; and (ii) substantial inertia is an inherent property of these problems, which can only be captured using long-term scenarios.

The Integrated Model to Assess the Global Environment (IMAGE) (Stehfest et al., 2014) is one of such IAMs. IMAGE is structured around key global sustainability problems (Fig. 1). Similar to other IAMs, it contains two main subcomponents: i.e. (i) the human system, describing the long-term development of human activities relevant for sustainable development issues, and (ii) the earth system, describing changes in the natural environment. The two systems are coupled via the impact of human activities on the environment, and via the impacts of environmental change back on the human system.

This paper describes the IMAGE-Global Nutrient Model (GNM), which simulates the fate of nitrogen (N) and phosphorus (P) in surface water arising from concentrated point sources (wastewater from urban and rural populations, and industrial wastewater), and from dispersed (non-point) sources such as agricultural production systems with its fertilizer application and manure management, and natural ecosystems. This global-scale model focuses is on prolonged historical periods for testing output results, and

Coupling global models for hydrology and nutrient loading

A. H. W. Beusen et al.

Title Page

Abstract

Introduction

Conclusions

References

Tables

Figures



Back

Close

Full Screen / Esc

Printer-friendly Version

Interactive Discussion



future scenarios to analyze consequences of future global change. IMAGE-GNM uses the grid-based global hydrological model PCR-GLOBWB (Van Beek et al., 2011) to quantify water stores and fluxes, volume, surface area, and thus depth of water bodies, and water travel time. IMAGE-GNM takes spatially explicit input from the IMAGE land model, including land cover and the annual surface N balance from inputs such as biological N fixation, atmospheric N deposition and the usage of synthetic N fertilizer and animal manure. The IMAGE-GNM model comprises processes such as N removal due to crop harvesting, hay and grass-cutting and grazing (Fig. 1). Starting from the soil nutrient budgets, IMAGE-GNM simulates the outflow of nutrients from the soil in combination with emissions from point sources and direct atmospheric deposition to determine the nutrient load to surface water and its fate during transport via surface runoff. It furthermore tracks nutrient transport in groundwater, riparian zones, lakes and reservoirs and in-stream biogeochemical retention processes. Earlier versions of parts of this model, particularly for the nutrient flows towards surface water, have been described previously for N (Van Drecht et al., 2003; Bouwman et al., 2013a), where the retention of N in streams, rivers, lakes and reservoirs was represented by a single, global coefficient. A first step to improve these approaches was the coupling of IMAGE with a hydrological model at the global scale to analyze N retention as pioneered by Wollheim et al. (2008b). Following Wollheim et al. (2008b), the version of IMAGE-GNM presented here uses the nutrient spiraling approach (Newbold et al., 1981) to describe in-stream retention of both total N and total P with a yearly time step.

Various other model approaches exist (Bouwman et al., 2013c). The widely-used regression models lump the combined effects of nutrient transformations in the continental system into a set of parameters and equations which can ultimately predict the drainage basin discharge of various geochemical species (e.g. dissolved inorganic and organic, and particulate N, P, C, Seitzinger et al., 2005, 2010; Mayorga et al., 2010). For our purposes, these lumped regression models have limited value, because they both ignore spatial variability of sources and sinks within river basins, and amalgamate all processes in the river continuum. They thus cannot elucidate the nonlinear behav-

Coupling global models for hydrology and nutrient loading

A. H. W. Beusen et al.

Title Page

Abstract

Introduction

Conclusions

References

Tables

Figures



Back

Close

Full Screen / Esc

Printer-friendly Version

Interactive Discussion



ior that results from the interplay between nutrient sources and biogeochemical processes. The SPARROW (SPATIally Referenced Regression On Watershed attributes, Smith et al., 1997; Alexander et al., 2008) model and similar hybrid approaches correlate measured stream nutrient fluxes with spatial data on nutrient sources and landscape characteristics. However, the disadvantage of such an approach is that only a limited time period is covered, while many scientific questions regarding the anthropogenic pressures on the nutrient cycles require prolonged time periods. On the other extreme, there is a range of continuous or event-based distributed watershed-scale models available which simulate all the components of a landscape, with the hydrology as the basis of calculations. An inventory of such mechanistic models was presented by (Borah and Bera, 2003). These models usually focus on N while ignoring P and tend to require extensive data that may be difficult to obtain at the spatiotemporal scales of human-climate interactions, and thus are less appropriate to implement in IMAGE-GNM.

In summary, IMAGE-GNM is a global, spatially explicit model which uses hydrology as the basis for describing N and P delivery to surface water and in-stream transport and retention. It is part of the IAM IMAGE, and used to study the impact of multiple environmental changes over timeframes which capture the mutual feedbacks between humanity and the Earth system. In this manuscript, we compare the model behavior against observations for a number of rivers, and test its sensitivity to a range of model parameter variations to analyze the impact of changing nutrient loading, climate and hydrology.

2 Model description

2.1 General aspects

The IMAGE model utilizes historical data for testing the model behavior, and projections to describe direct and indirect drivers of future global environmental change. Most of

Coupling global models for hydrology and nutrient loading

A. H. W. Beusen et al.

Title Page

Abstract

Introduction

Conclusions

References

Tables

Figures



Back

Close

Full Screen / Esc

Printer-friendly Version

Interactive Discussion



these drivers (such as technology and lifestyle assumptions) are used as input in various subcomponents of IMAGE such as GNM (Fig. 1). Clearly, the exogenous assumptions made on these factors need to be consistent. To ensure this, so-called storylines are used, brief descriptions about how the future may unfold, that can be used to derive internally consistent assumptions for the main driving forces of each IMAGE module. Important categories of scenario drivers include demographic factors, economic development, lifestyle, and technology change. Among these, population and economic development form a special category as they can be dealt with in a quantitative sense as exogenous model drivers.

The geographical resolution of IMAGE 3.0 is 26 socio-economic world regions (Steffest et al., 2014). These regions are selected given their relevance for global environmental problems and a relatively high degree of internal coherence. In the Earth system, the key geographic scale is a $0.5 \times 0.5^\circ$ grid for plant growth, land cover, carbon, nutrient and water cycles. In terms of temporal scale, both systems are run at an annual time step, focusing on long-term trends to capture important inertia aspects of global environmental problems such as simultaneously changing climate and various human activities. Within the Earth system, much shorter time steps are used for water, crop and vegetation modeling. For many applications the IMAGE model deliberately runs over the historical period of 1970 until present day in order to test model dynamics against key historical trends and then up to 2050, depending on the focus of the analysis. IMAGE-GNM is integrated in the IMAGE model framework, as it has to account for all the drivers that determine the nutrient emissions from point and diffuse sources and their transport. IMAGE-GNM is therefore a distributed model with temporal resolution of 1 year, and a spatially explicit resolution of 0.5 by 0.5° .

IMAGE provides land cover and soil budgets for N and P and IMAGE-GNM outputs the nutrient delivery to surface water via surface and subsurface runoff (see Sect. 2.4.2 and 2.4.3) (Fig. 2). IMAGE distinguishes grid cells with natural vegetation or agriculture. Within each agricultural grid cell IMAGE computes distributions of seven crop groups that are aggregated in IMAGE-GNM to larger groups (pastoral grassland, grassland in

mixed systems, wetland rice, legumes and upland crops). The soil N budget (N_{budget}) is calculated for each of these groups and then aggregated to the level of 0.5 by 0.5° grid cells for individual years as follows:

$$N_{\text{budget}} = N_{\text{fix}} + N_{\text{dep}} + N_{\text{fert}} + N_{\text{man}} - N_{\text{withdr}} - N_{\text{vol}} \quad (1)$$

Where N_{fix} is biological N fixation (kg), N_{dep} is atmospheric N deposition (kg), N_{fert} is application of synthetic N fertilizer (kg), N_{man} is animal manure (kg), N_{withdr} is N removal from via crop harvesting, hay and grass cutting, and grass grazed by animals (kg), and N_{vol} is ammonia (NH_3) volatilization (kg). The N budget is prone to erosion, leaching or denitrification, or can accumulate in the soil. Following the approach of Bouwman et al. (2013e, a), the P budget is assumed to depend on erosion, and soil accumulation. P inputs for the soil budget are fertilizer and animal manure, and outputs are crop and grass withdrawal.

The data exchange between PCR-GLOBWB and IMAGE-GNM is presented in Fig. 2. Spatial land cover distributions from IMAGE and global climate data from ERA-40 re-analysis (Uppala et al., 2005) are used in PCR-GLOBWB for computing the water balance, runoff and discharge for each year. For each grid cell, IMAGE-GNM provides the delivery of N and P to water bodies via diffuse sources (surface runoff, shallow and deep groundwater, riparian zones) and point sources (wastewater) (Figs. 3 and 4). Grid cells receive water with dissolved and suspended N and P from upstream grid cells, and from diffuse and point sources within the grid cell. In each grid cell, N and P retention in a water body is calculated on the basis of the residence time of the water and nutrient uptake velocity, and subsequently, water and nutrients are transported to downstream grid cells. Discharge is routed to obtain the accumulated water and nutrient flux in each grid cell, through streams, rivers, lakes, wetlands and reservoirs (Fig. 4).

The various submodels for hydrology, spatially explicit nutrient delivery patterns and in-stream retention (Fig. 3), used within IMAGE-GNM are parameterized independently. Furthermore, these parameters are not calibrated in order to better understand the

Coupling global models for hydrology and nutrient loading

A. H. W. Beusen et al.

Title Page

Abstract

Introduction

Conclusions

References

Tables

Figures



Back

Close

Full Screen / Esc

Printer-friendly Version

Interactive Discussion



model behavior, identify the lacunae in the data used, and discern the influence of the various processes considered in the model. Instead, the sensitivity of different model outputs to changes in values of input data and model parameters is analyzed in order to explore our model and data.

Although part of the IMAGE framework, GNM can also be used as a stand-alone version, provided that all the input data are in the correct format. For example, land cover data and soil N budgets from various modelling groups could be used (Van Drecht et al., 2005; Fekete et al., 2011). Here we use an update of the nutrient data covering the period 1900–2000 presented by Bouwman et al. (2013e). Also, output from different hydrological models (e.g. Fekete et al., 2011; Alcamo et al., 2003) could be compared.

IMAGE-GNM is written in Python 2.7 code. The complete code is available in the Supplement.

2.2 Hydrology

2.2.1 Water balance

The land surface in PCR-GLOBWB is represented by a topsoil (0.3 m thick or less) and a subsoil (1.2 m thick or less). Precipitation falls as rain if air temperature exceeds 0 °C, and as snow otherwise. Snow accumulates on the surface, and melt is temperature controlled. Potential evapotranspiration is broken down into canopy transpiration and bare-soil evaporation, which are reduced to an actual evapotranspiration rate based on soil moisture content. Vertical transport in the soil column arises from percolation or capillary rise, depending on the vertical hydraulic gradient present between these layers.

Precipitation and temperature are from New et al. (2000) and downscaled to daily values using the ERA-40 reanalysis (Uppala et al., 2005). Precipitation and temperature were fed directly into the model whereas secondary variables (vapor pressure, wind speed, cloud cover,) were used to compute reference potential evapotranspiration using the Penman–Monteith equation according to guidelines of the Food and Agricul-

Coupling global models for hydrology and nutrient loading

A. H. W. Beusen et al.

Title Page

Abstract

Introduction

Conclusions

References

Tables

Figures



Back

Close

Full Screen / Esc

Printer-friendly Version

Interactive Discussion



Coupling global models for hydrology and nutrient loading

A. H. W. Beusen et al.

Title Page

Abstract

Introduction

Conclusions

References

Tables

Figures



Back

Close

Full Screen / Esc

Printer-friendly Version

Interactive Discussion



large streams, where riparian zones are bypassed. Although riparian zones may only account for a small percentage of the drainage basin, they are critical control points for groundwater and N fluxes within many basins (Vidon and Hill, 2006). Riparian zones along small streams have long ecotone lengths within drainage networks, and may process groundwater N at faster rates than larger nearby water bodies (Bouwman et al., 2013a).

2.2.2 Vegetation and land cover

Vegetation effects are taken into account by partitioning the land surface by fraction into different types. Similarly, spatial variations in soil properties can be accounted for by considering effective values for each of these vegetation types. Soil characteristics are assumed to be constant under changing land cover, except for soil total available water capacity (*tawc*); the relative distribution of *tawc* varies with changing root depth distributions based on Canadell et al. (1996). All other soil parameters are from the FAO Digital Soil Map of the World (FAO, 1991) and the Wise data from the International Soil Reference and Information Center (ISRIC)-World Soil Information (Batjes, 1997, 2002). Lithological properties (such as hydraulic conductivity) are derived from a global lithological map (Dürr et al., 2005).

Similar to earlier implementations of PCR-GLOBWB, vegetation parameters are taken from the Olson classification of the Global Land Cover Characterization (GLCC) dataset with a resolution of 30 arc seconds and values assigned using the parameter dataset of Hagemann et al. (1999). The parameterization is adjusted to the reconstruction of agricultural land cover for 1900–2000 with 5-year time steps derived from the IMAGE model (Bouwman et al., 2013d) based on historical data (Klein Goldewijk et al., 2010) in order to achieve consistency between the simulated hydrology and imposed land use.

The land cover reconstruction for the 20th century specifies the fractions of arable land and grassland within each 0.5 by 0.5° grid cell. To combine this information with the Olson classification, three separate maps at the original resolution of 30 arc seconds

were created, including (i) Olson classes that were assumed to represent semi-natural vegetation and that were spatially extrapolated per Holdridge Life Zone (Holdridge, 1967); (ii) Olson classes representing cropland; (iii) Olson classes representing grassland.

For the reconstructed land cover under the two agriculturally managed conditions, i.e., crops and pasture, all 30 arc seconds cells within a 0.5 by 0.5° cell are ranked in order of decreasing suitability from 0 to 1. This is achieved by first delineating their current extent in the GLCC and ranking on the basis of slope, computed from the Hydro1k database (Verdin and Greenlee, 1996). Next, the adjoining cells are ranked on the basis of the slope parallel distance starting from the delineated areas. These rank orders are then normalized, values near zero indicating the most suitable locations, one indicating the poorest locations, and used to match the IMAGE derived fractions for each 0.5 by 0.5° cell. In this procedure, cropland has priority, followed by grassland. Any remaining areas are subsequently filled with semi-natural vegetation types. On the basis of the resulting patched land cover, the land cover parameterization for PCR-GLOBWB was then derived.

2.2.3 Drainage network

Drainage density is computed from the Hydro1k dataset (Verdin and Greenlee, 1996). The drainage network is based on the DDM30 flow direction map of (Döll and Lehner, 2002) and the lake characteristics taken from the Global Lakes and Wetlands Database version 1 (GLWD1) product (Lehner and Döll, 2004). Reservoirs are from the Global Reservoir and Dam (GRaND) database (Lehner et al., 2011) and introduced dynamically on the basis of the reported construction year.

The water level in lakes is constant, as the through flow will increase with increasing discharge. The water travel time is determined by the discharge and the volume of the water body. Assuming that flooding occurs once a year and that all river discharge follows the main channel, the travel time in a river with floodplains is determined as

Coupling global models for hydrology and nutrient loading

A. H. W. Beusen et al.

Title Page

Abstract

Introduction

Conclusions

References

Tables

Figures



Back

Close

Full Screen / Esc

Printer-friendly Version

Interactive Discussion



follows:

$$\tau = \frac{V}{Q - Q_f} \quad (6)$$

Where τ is the travel time (year), V is the volume of the water body (including river bed) (m^3), Q is the discharge ($\text{m}^3 \text{yr}^{-1}$) and Q_f is the discharge into the flooded area ($\text{m}^3 \text{yr}^{-1}$). While the simulated discharge includes the regulating effect of reservoirs, consumptive water use has not been included as it is difficult to identify its source (groundwater, surface water) and to quantify its spatial distribution with certainty.

Water bodies such as lakes and reservoirs can extend over several 0.5 by 0.5° grid cells and are included if their volume exceeds that of the channel within a cell. Where more than one reservoir is located within the same grid cell, they are merged and the combined storage and volume assigned to the dominant reservoir. At the start of the simulation, in 1901, 107 out of a total of 132 reservoirs of the GRaND dataset are included as 88 spatially individual water bodies, corresponding to 78 % of the reported total volume of 16.4 km^3 . For 2000, 5595 out of a total of 6369 reservoirs are included as 3507 spatially individual water bodies, corresponding to 98 % of the reported total volume of 5848.4 km^3 . No demand is imposed on the reservoirs and by default they are assigned the purpose of hydropower generation. In absence of pricing generation at the global scale (Haddeland et al., 2006; Adam and Lettenmaier, 2008), this results in an operation that maximizes the available potential energy. In this case, this conforms with 75 % of the maximum storage capacity in absence of detailed global data. The remaining 25 % are reserved to buffer inflow for flood control purposes. Reservoir release is linearly scaled to storage when reservoir storage falls below 30% of the available capacity. This reduced outflow also results in a realistic, gradual filling of reservoirs after completion of dam construction.

Coupling global models for hydrology and nutrient loading

A. H. W. Beusen et al.

Title Page

Abstract

Introduction

Conclusions

References

Tables

Figures



Back

Close

Full Screen / Esc

Printer-friendly Version

Interactive Discussion



2.3 Nutrient delivery to surface water

Surface and subsurface runoff are calculated from the soil N and P budgets on the basis of the hydrological flows provided by PCR-GLOBWB. Other nutrient sources that are directly delivered to surface water included in IMAGE-GNM are wastewater from urban areas, aquaculture, allochthonous organic matter, weathering and atmospheric deposition.

2.3.1 Nutrients directly delivered to surface water

N and P inputs from wastewater for the 20th century are from Morée et al. (2013), and those from freshwater aquaculture are calculated using the country-scale model estimates of Bouwman et al. (2013b) for finfish and Bouwman et al. (2011) for shellfish using data for the period 1950–2000 from FAO (2013); data indicate that prior to 1950 aquaculture production was negligible. N and P emissions from aquaculture are allocated within countries using three weighing factors, i.e. population density, presence of surface water bodies, and mean annual air temperature. For population density, all grid cells with no inhabitants and those with more than 10 000 inhabitants km⁻² are excluded; around an optimum density of 1000 inhabitants km⁻², a steep parabolic function on the left and less steep on the right are used to calculate the weighing. Lakes, reservoirs, rivers and wetlands have the maximum weight for water bodies, and floodplains and intermittent lakes only half of that; all other types have a weight of zero. Grid cells with mean annual air temperature < 0 °C are excluded for aquaculture. The three weighing factors are combined by multiplication to obtain the overall weight [0,1]. Then all grid cells with overall probability < 10 % are excluded for aquaculture, yielding the map for allocation for all years. Subsequently, the country production for shellfish and finfish are allocated separately. Grid cells with fish production less than a threshold are excluded for that particular year, and the remaining grid cells are used to allocate the N and P emissions from shellfish and finfish based on the weighing map.

Coupling global models for hydrology and nutrient loading

A. H. W. Beusen et al.

Title Page

Abstract

Introduction

Conclusions

References

Tables

Figures

◀

▶

◀

▶

Back

Close

Full Screen / Esc

Printer-friendly Version

Interactive Discussion



Allochthonous organic matter input to surface water is an important flux in the global C cycle (Cole et al., 2007). This could be an important source of nutrients, but so far its magnitude has not been investigated. Here, estimates of NPP from IMAGE for wetlands and floodplains are used. Part of annual NPP is assumed to be deposited in the water during flooding, and where flooding is temporary, the litter from preceding periods is assumed to be available for transport in the flood water. The ratio of litter to belowground inputs of organic matter ranges from 30 : 70 to 70 : 30 (Trumbore et al., 1995; Vogt et al., 1986); 50 % of total NPP is assumed to end in the surface water. N and P inputs to the water are estimated based on a C : N ratio of 100 and a C : P ratio of 1200 (Vitousek, 1984; Vitousek et al., 1988).

The calculation of P release from weathering is based on a recent study (Hartmann et al., 2014) which uses the lithological classes distinguished by Dürr et al. (2005). The lithological classes are available on a 5 by 5 min resolution, hence the weighted average P concentration within each 0.5 by 0.5° grid cell is calculated, and the $P_{\text{RivLoadWeath}}$ (kg P yr⁻¹) is computed as follows:

$$P_{\text{RivLoadWeath}} = 10^{-3} C_{\text{PWeath}} q_{\text{tot}} A_{\text{gridcell}} \text{SS}_{\text{corr}} \exp \left(-\frac{E_{\text{a,w}}}{R} \left(\frac{1}{K} - \frac{1}{284} \right) \right) \quad (7)$$

where C_{PWeath} (gm⁻³) is the background concentration specified for each lithological class (Table 1) and derived from river runoff data, q_{tot} is the total runoff (myr⁻¹) and A_{gridcell} is the land area (m²) in the grid cell considered, SS_{corr} is a correction factor for soil shielding, and $E_{\text{a,w}}$ is the activation energy (J mol⁻¹) (Table 1), K the local mean annual air temperature (Kelvin) and R the molar gas constant (8.3144 J mol⁻¹ K⁻¹). The soil shielding correction SS_{cor} is a correction factor of 0.1 leading to a 90 % reduction for FAO soil units (FAO/Unesco, 1988) Ferralsols, Acrisols, Nitosols, Lixisols, Gleysols (soils with hydromorphic properties) and Histosols (organic soils). For all other soils $\text{SS}_{\text{cor}} = 1$ (no reduction). With this approach, regions with the same lithology but with more precipitation have higher P weathering losses than regions in dry climates.

Atmospheric N deposition to water bodies is from the ensemble of reactive-transport models for the year 2000 (Dentener et al., 2006), and the years before that were made by scaling the deposition with grid-based emissions of ammonia (Bouwman et al., 2013d). The deposition in floodplains, wetlands and river channels is ignored, because it is already part of the soil N budget, and does not need to be accounted for in periods of flooding.

2.3.2 Surface runoff

IMAGE-GNM distinguishes two surface runoff mobilization pathways for nutrients, i.e. losses from recent nutrient applications in the form of fertilizer, manure or organic matter ($N_{\text{sro,rec}}$, $P_{\text{sro,rec}}$) (Hart et al., 2004), and a “memory” effect ($N_{\text{sro,mem}}$, $P_{\text{sro,mem}}$) related to long-term historical changes in soil nutrient inventories (McDowell and Sharp-ley, 2001; Tarkalson and Mikkelsen, 2004):

$$N_{\text{sro}} = N_{\text{sro,rec}} + N_{\text{sro,mem}} \quad (8)$$

Estimates of soil loss by rainfall erosion from Cerdan et al. (2010) based on a large database of measurements were used as a basis for calculating $P_{\text{sro,mem}}$ and $N_{\text{sro,mem}}$. The approach presented by Cerdan et al. (2010) based on slope, soil texture and land cover type were used to estimate country aggregated soil-loss rates for arable land, grassland and natural vegetation. Soil loss from peat soils was assumed to be low (equal to fine texture). These estimates were then adjusted to obtain the mean erosion loss estimates for Europe (360 t of soil per km² for arable fields, 40 t per km² for grassland and 15 t per km² for natural vegetation). The model was then applied to all grid cells of the world. For global grasslands this yields an erosion rate of 60 t of soil per km² which exceeds the European rate by 50 % due to larger erosivity of grasslands in especially tropical and (semi-)arid climates.

As the model keeps track of all inputs and outputs in the soil P budget, the actual P content can be calculated. The initial P stock for the year 1900 in the top 30 cm is taken from Yang et al. (2010). All inputs and outputs of the soil balance are assumed to occur

Coupling global models for hydrology and nutrient loading

A. H. W. Beusen et al.

Title Page

Abstract

Introduction

Conclusions

References

Tables

Figures

⏪

⏩

◀

▶

Back

Close

Full Screen / Esc

Printer-friendly Version

Interactive Discussion



Coupling global models for hydrology and nutrient loading

A. H. W. Beusen et al.

Title Page

Abstract

Introduction

Conclusions

References

Tables

Figures

◀

▶

◀

▶

Back

Close

Full Screen / Esc

Printer-friendly Version

Interactive Discussion



in the top 30 cm; the model replaces P enriched or depleted soil material lost at the surface by erosion with fresh soil material (with the initial soil P content) at the bottom. For N the soil organic C content, which is assumed to be constant over time, is used as a basis to calculate N in eroded soil material using land-use specific C : N ratios (soil C : N for arable land 12, for grassland 14 and for soils under natural vegetation 14) (based on Batjes, 1996; Guo and Gifford, 2002; McLauchlan, 2006; Brady, 1990). Hence, with changing land use, the N content in soil erosion loss will also change.

$P_{\text{sro,rec}}$ and $N_{\text{sro,rec}}$ are calculated from the N and P input terms (Eq. 1) on the basis of f_{qsro} , (Eq. 4). For N the equation is:

$$N_{\text{sro,rec}} = f_{\text{cal}} f_{\text{qsro}} N_{\text{inp}}(\text{landuse}) \quad (9)$$

where f_{cal} is a correction coefficient of 0.3 to match the N runoff results of the Miterra model (Velthof et al., 2009, 2007).

2.3.3 Subsurface nitrogen removal and delivery

Subsurface transport of P is neglected, as P is easily absorbed by soil minerals; leaching of P may occur only in P-saturated soils with long histories of heavy over-fertilization; below the saturated soil layer, P will be absorbed to the minerals occurring there, which are low in P. All the positive values of the soil N budget (Eq. 1) are subjected to leaching. Leaching from the top 1 m of soil (or less for thinner soils) is a fraction of the soil N budget excluding the N lost by surface runoff ($f_{\text{leach,soil}}$, Van Drecht et al., 2003):

$$N_{\text{leach,soil}} = f_{\text{leach,soil}} (N_{\text{budget}} - N_{\text{sro}}) \quad (10)$$

where $f_{\text{leach,soil}}$ is:

$$f_{\text{leach,soil}} = [1 - \text{MIN}[(f_{\text{climate}} + f_{\text{text}} + f_{\text{drain}} + f_{\text{soc}}), 1]] f_{\text{landuse}} \quad (11)$$

The fraction of N lost by denitrification ($f_{\text{den,soil}}$) complements $f_{\text{leach,soil}}$ ($f_{\text{den,soil}} = 1 - f_{\text{leach,soil}}$). f_{text} , f_{drain} , and f_{soc} represent factors that address the soil texture, aeration,

Coupling global models for hydrology and nutrient loading

A. H. W. Beusen et al.

Title Page

Abstract

Introduction

Conclusions

References

Tables

Figures

◀

▶

◀

▶

Back

Close

Full Screen / Esc

Printer-friendly Version

Interactive Discussion



soil organic carbon (C) content, respectively (Table 2). Fine-textured soils are more susceptible to reach and maintain anoxia, which favors denitrification, as they are characterized by higher capillary pressures and hold water more tightly than sandy soils. Denitrification rates tend to be higher in poorly drained than in well-drained soils (Bouman et al., 1993). The soil organic C content is used as a proxy for the C supply, which can have a direct impact on the soil oxygen concentrations. f_{landuse} is the land use effect on leaching, where arable land has a value of 1, and grassland and natural vegetation a value of 0.36 (Keuskamp et al., 2012).

The factor f_{climate} (–) combines the effects of temperature, water residence time, and NO_3^- in the root zone on denitrification rates. f_{climate} is the product of the temperature effects on denitrification (f_K , –) and the mean annual residence time of water and NO_3^- in the root zone ($T_{r,\text{so}}$, yr):

$$f_{\text{climate}} = f_K T_{r,\text{so}} \quad (12)$$

The temperature effect f_K follows the Arrhenius equation (Firestone, 1982; Shaffer et al., 1991; Kragt et al., 1990):

$$f_K = 7.94 \times 10^{12} \exp\left(\frac{-E_{a,d}}{RK}\right) \quad (13)$$

where $E_{a,d}$ is the activation energy ($74\,830 \text{ J mol}^{-1}$), K the mean annual temperature (Kelvin) and R is the molar gas constant ($8.3144 \text{ J mol}^{-1} \text{ K}^{-1}$). $T_{r,\text{so}}$ is calculated via:

$$T_{r,\text{so}} = \frac{tawc}{q_{\text{eff}}} \quad (14)$$

where $tawc$ (m) is the total available water capacity for the top 1 m (or less if thinner) of soil and q_{eff} is described in Eq. (5). Based on the negligible retardation of NO_3^- , the water and NO_3^- residence times are assumed to be the same. Soils used for agricultural

crops in dry regions with $T_{r,so} < 1$ receive a $T_{r,so}$ value of 1.0 assuming that irrigation is required to grow crops in these locations.

Arid regions under grassland or natural vegetation have long residence times according to Eq. (14), and results in values of $f_{climate}$ and $f_{den,soil}$ equal to one, implying that denitrification removes all the N. This representation is not realistic, since N can accumulate in the vadose zone below the root zone as nitrate (Walvoord et al., 2003), and can escape via surface runoff, ammonia-N volatilization, and denitrification (Peterjohn and Schlesinger, 1990). It is not possible to quantify the relative contribution of each process (Peterjohn and Schlesinger, 1990), but it is clear that only a negligible part of N surpluses in arid climates is lost by denitrification. Denitrification was thus neglected from the fate of N surplus in soils receiving an annual precipitation of < 3 mm and overlain with grasslands and natural vegetation. For the year 2000, N surplus in the 3100 Mha of global arid lands was 20 Tg.

The N concentration C_N in the excess water leaching from the root zone (depth $z = 0$) is represented by the ratio of leached N over q_{eff} (Eq. 5):

$$C_N(z = 0) = \frac{N_{leach}}{q_{eff}} \quad (15)$$

The groundwater N concentration varies according to the historical year of infiltration into the saturated zone and the denitrification (including anammox) during groundwater advection (Böhlke et al., 2002; Van Drecht et al., 2003). The time available for denitrification is represented by the mean travel time $T_{r,aq}$, which is the ratio of the specific groundwater volume and the water recharge:

$$T_{r,aq}(t) = \text{MIN} \left[\frac{\rho D}{q_{inflow}(t)}, 1000 \right] \quad (16)$$

where D is aquifer thickness (m) and can either be for shallow groundwater ($D_{sgrw} = 5$ m) or for deep groundwater ($D_{dgrw} = 50$ m) following Meinardi (1994). q_{inflow} is either the shallow groundwater recharge (q_{int} , m y^{-1}) or deep groundwater recharge, (q_{gwb} ,

Coupling global models for hydrology and nutrient loading

A. H. W. Beusen et al.

Title Page

Abstract

Introduction

Conclusions

References

Tables

Figures



Back

Close

Full Screen / Esc

Printer-friendly Version

Interactive Discussion



m y^{-1}). The vertical drainage of the shallow groundwater feeds the deep groundwater (Fig. 3). The vertical flow distribution for the shallow system is uniform so the travel time can be equated to the mean travel time. In contrast travel times for lateral flows to the fluvial system vary considerably. The travel time distribution for lateral flow in a vertical cross section is represented by (Meinardi, 1994):

$$g_{\text{age}}(z) = -T_{\text{r,aq}} \ln(1 - (z/D)) \quad (17)$$

where g_{age} (yr) is the age of groundwater at a specific depth, and z (m) is the depth in the aquifer (i.e. $z = 0$ at the top of the aquifer and $z = D$ at the bottom of the aquifer),

Denitrification takes place during transport in the shallow system along the various flow paths in a homogeneous and isotropic aquifer, drained by parallel rivers or streams. IMAGE-GNM simulates the effects of denitrification in N concentrations at time t and depth z ($C_{\text{N}}(t, z)$) through a first order degradation reaction, leading to an exponential decay equation for the nitrogen concentration:

$$C_{\text{N}}(t, z) = C_{\text{N}}(t - g_{\text{age}}(z), 0) e^{-k g_{\text{age}}(z)} \quad (18)$$

where t is time and the decay rate k is obtained via the half-life of nitrate ($dt50_{\text{den}}$) due to denitrification:

$$k = \frac{\ln(2)}{dt50_{\text{den}}} \quad (19)$$

Lithology can have a direct effect on denitrification, and thus $dt50_{\text{den}}$ (Dürr et al., 2005). Silici-clastic material exhibits low $dt50_{\text{den}}$ values of 1 y^{-1} , whereas alluvial material has $dt50_{\text{den}}$ values of 2 y^{-1} and all other lithology classes have a $dt50_{\text{den}}$ value of 5 y^{-1} (Table 1). The N concentration in water percolating to deep groundwater represents the outflow from shallow groundwater. IMAGE-GNM assumes that denitrification is absent in deep groundwater. Although denitrification could occur in organic matter- and/or pyrite-rich deep aquifers, denitrification measurements in the literature have a bias toward high rates (Green et al., 2008), which makes their global assessment difficult.

Coupling global models for hydrology and nutrient loading

A. H. W. Beusen et al.

Title Page

Abstract

Introduction

Conclusions

References

Tables

Figures

◀

▶

◀

▶

Back

Close

Full Screen / Esc

Printer-friendly Version

Interactive Discussion



Following Beusen et al. (2013), nitrogen transported through submarine groundwater discharge (SGD) is excluded from the delivery to rivers and other water bodies. This assumption is justified, since, only 10 % of the gridded map could contribute to SGD. The remaining aquifer discharge in the grid box goes towards streams and rivers.

While urban areas can have an effect in the N loss to the environment (e.g. Foppen, 2002; Wakida and Lerner, 2005; Van den Brink et al., 2007; Nyenje et al., 2010), the total urbanized land represents 0.3 % of the total land area (Angel et al., 2005), and thus it is neglected from the model. The median NH_4 concentration in groundwater of 25 European aquifers is 0.15 mg L^{-1} (Shand and Edmunds, 2008), which represents a small part (0.7–1.2 %) of the nitrogen concentration (EEA, 2013), and thus NH_4 in groundwater is also neglected.

2.3.4 N transport and removal in riparian zones

Modelling geochemical processes in riparian zones requires a detailed hydrological and geographical information at very high spatial scales, since, even at 0.1 km resolution the topography of the riparian area cannot be adequately assessed (Vidon and Hill, 2006). IMAGE-GNM therefore uses a conceptual approach.

In riparian zones, denitrification rates depend highly on the local pH (Simek and Cooper, 2002; Knowles, 1982), temperature, water saturation, NO_3^- availability and soil organic carbon availability. Previous laboratory studies of pure cultures have shown that denitrification is maximized at a pH of 6.5 to 7.5, and decreases at both low (below 4) and high (above 10) pH values (van Cleemput, 1998; Van den Heuvel et al., 2011).

As with soil denitrification, riparian zone denitrification is calculated using dimensionless reduction factors and is based on the characteristics of the groundwater flow, soil and climate. Heterotrophic denitrification is assumed to be highest at $\text{pH} > 7$ (van den Heuvel et al., 2010). A pH reduction factor $f_{\text{denpH,rip}}$ is then used to reduce the value with decreasing pH, such that $f_{\text{denpH,rip}} = 1$ at $\text{pH} > 7$ and 0 at $\text{pH} < 3$ (Fig. 5).

$$N_{\text{den,rip}} = f_{\text{den,rip}} N_{\text{in}} \quad (20)$$

where N_{in} is the nitrogen that enters the riparian zone from the shallow groundwater.

$$f_{den,rip} = \text{MIN}[(f_{climate} + f_{text} + f_{drain} + f_{soc}), 1]f_{denpH,rip} \quad (21)$$

where $f_{climate}$ is the product of f_K (Eq. 13) and the water (and NO_3^-) travel time through the riparian zone ($T_{r,rip}$). $T_{r,rip}$ depends on the thickness of the riparian zone ($D_{rip} \leq 0.3$ m, depending on the soil thickness), on the available water capacity for the top 1 m of the riparian zone ($tawc$), and on the flow of water entering the riparian zone from the shallow groundwater (q_{int}):

$$T_{r,rip} = \frac{D_{rip} tawc}{q_{int}} \quad (22)$$

2.4 In-stream nutrient retention

Three processes contribute to N retention, i.e. denitrification, sedimentation and up-take by aquatic plants. Denitrification is generally the major component of N retention (Saunders and Kalf, 2001). P is removed by sedimentation and sorption by sediment (Reddy et al., 1999). Retention in a grid cell is calculated as a first order approximation according to:

$$R = 1 - \exp\left(-\frac{v_{f,E}}{H_L}\right) \quad (23)$$

Where R is the fraction of the nutrient load that is removed (-), v_f is the net uptake velocity (m yr^{-1}), E is the nutrient considered (N or P), H_L is the hydraulic load (m yr^{-1}) obtained from:

$$H_L = \frac{D}{\tau} \quad (24)$$

Where D is the depth of the water body (m), τ is the residence time (yr); τ is calculated from the volume V (m^3) of the water body and the discharge Q ($\text{m}^3 \text{ yr}^{-1}$):

$$\tau = \frac{V}{Q} \quad (25)$$

for all water bodies except for river channels and floodplains where the discharge Q is reduced by the water volume in the floodplains (see Eq. 6). In this approach hydrological (defined by H_L) and biological and chemical factors (defined by v_f) controlling retention are isolated, assuming first order kinetics is applicable (i.e., areal uptake changes linearly with concentration).

Net uptake velocity is different for each element E (N or P). For N, the basic value for all water body types of 35 myr^{-1} taken from (Wollheim et al., 2006, 2008b) is modified based on temperature and N concentration:

$$v_{f,N} = 35f(t)f(C_N) \quad (26)$$

Where t is annual mean temperature ($^{\circ}\text{C}$) and C_N is the N concentration in the water. $f(C_N)$ describes the effect of concentration on denitrification as a result of electron donor limitation in the case of high N loads; the results of Mulholland et al. (2008) were mimicked by assuming a decrease of $f(C_N)$ from a value of 7.2 at $C_N = 0.0001 \text{ mg L}^{-1}$ to 1 for $C_N = 1 \text{ mg L}^{-1}$, a further decrease to 0.37 for $C_N = 100 \text{ mg L}^{-1}$ and constant at higher concentrations.

The temperature effect $f(t)$ is calculated as:

$$f(t) = \alpha^{t-20}(t-20) \quad (27)$$

Where $\alpha = 1.0717$ for N (following Wollheim et al., 2008b, and references therein) and $\alpha = 1.06$ for P (following Marcé and Armengol, 2009).

For P, the basic value for v_f of 44.5 myr^{-1} taken from Marcé and Armengol (2009) is used for all water body types, with a modification based on temperature:

$$v_{f,P} = 44.5f(t) \quad (28)$$

The drainage network of PCR-GLOBWB represents streams and rivers of Strahler order (Strahler, 1957) six and higher. The parameterization of lower order streams follows the approach presented by Wollheim et al. (2008a). A globally uniform subgrid

Coupling global models for hydrology and nutrient loading

A. H. W. Beusen et al.

Title Page

Abstract

Introduction

Conclusions

References

Tables

Figures



Back

Close

Full Screen / Esc

Printer-friendly Version

Interactive Discussion



river network is included for all grid cells without lakes or reservoirs. It is assumed that PCR-GLOBWB has one river of order 6 in each grid cell, and all lower order rivers are lacking. The river network is then defined on the basis of stream length and basin area of the first order river. The mean length ratio R_L (–) is used to calculate the stream length of the next higher order the river according to:

$$L_n = L_1 R_L^{(n-1)} \quad (29)$$

with L_n being the stream length of order n (km); $L_1 = 1.6$ km. The drainage area ratio R_a (–) is used to calculate the basin area for higher order stream as follows:

$$A_n = A_1 R_a^{(n-1)} \quad (30)$$

Where A_n is basin area of order n in km^2 ; $A_1 = 2.6 \text{ km}^2$. With the stream number ratio R_b (–) the number of lower order streams is calculated as:

$$R_n = R_b^{(6-n)} \quad (31)$$

With R_n being the number of streams of order n in this grid cell and $R_b = 4.5$. The discharge for each stream is calculated with the runoff (q):

$$Q_n = q A_n C_Q \quad (32)$$

With the discharge of stream order n (Q_n) in $\text{m}^3 \text{ s}^{-1}$ and runoff in mm yr^{-1} and C_Q the unit conversion ($C_Q = 1000 / (3600 \times 24 \times 365)$). The midpoint discharge of a stream length of order n is calculated as

$$Q_{\text{mid},n} = Q_n + 0.5 Q_{n-1} \quad (33)$$

The width of the stream of order n is calculated as:

$$W_n = A(Q_{\text{mid},n})^B \quad (34)$$

GMDD

8, 7477–7539, 2015

Coupling global models for hydrology and nutrient loading

A. H. W. Beusen et al.

Title Page

Abstract

Introduction

Conclusions

References

Tables

Figures

◀

▶

◀

▶

Back

Close

Full Screen / Esc

Printer-friendly Version

Interactive Discussion



Where W_n = width (m), A is a constant ($A = 8.3$ m) and coefficient $B = 0.52$. It is now possible to calculate the hydrologic load (H_L) and thus the retention of the stream with according to:

$$H_L = \frac{C_{Q1} Q_{\text{mid},n}}{L_n W_n C_{Q2}} \quad (35)$$

5 With C_{Q1} being the conversion from seconds to years ($C_{Q1} = 3600 \times 24 \times 365$) and C_{Q2} the conversion from km to m (1000) and H_L in myr^{-1} . The local diffuse load in a grid cell is spatially uniformly distributed over the streams. Here, the fraction of the total stream length per order is used to calculate the distribution of the load. The direct load is allocated to stream order n as follows:

$$10 F_{d,n} = \frac{R_n L_n}{\sum_{i=1}^6 R_i L_i} \quad (36)$$

Where $F_{d,n}$ is the fraction of the total load which is direct input for streams of order n . The pathway of the outflow of the streams is determined according to a matrix $\mathbf{T}_{i,j}$ representing the fraction of the outflow of stream order i to stream order j , whereby $\mathbf{T}_{i,j} = 0.0$ for $i \geq j$. For $i < j$, $\mathbf{T}_{i,j}$ is calculated as follows:

$$15 \mathbf{T}_{i,j} = \frac{R_j L_j}{\sum_{k=i+1}^6 R_k L_k} \quad (37)$$

The calculation of the retention is performed for each stream order, starting with order $n = 1$, and is identical to the calculation of the PCR-GLOBWB schematization. The load of a stream is the sum of the direct load and the sum of the outflow from lower order streams.

Coupling global models for hydrology and nutrient loading

A. H. W. Beusen et al.

Title Page

Abstract

Introduction

Conclusions

References

Tables

Figures

◀

▶

◀

▶

Back

Close

Full Screen / Esc

Printer-friendly Version

Interactive Discussion



(Saltelli et al., 2000, 2004):

$$Y = \beta_0 + \beta_1 X_1 + \beta_2 X_2 \cdots + \beta_n X_n + e \quad (39)$$

where β_i is the so-called ordinary regression coefficient and e is the error of the approximation. The linear regression model can be evaluated using the coefficient of determination (R^2), which represents the Y variation as explained by $Y - e$. β_i depends on the scale and dimension of X_i , the sensitivity study can be normalized by rescaling the regression equation using of the standard deviations for Y and X (σ_Y and σ_{X_i} , respectively) and calculating the standardized regression coefficient (SRC_{*i*}):

$$\text{SRC}_i = \beta_i \frac{\sigma_{X_i}}{\sigma_Y} \quad (40)$$

SRC_{*i*} can take values in the interval $[-1, 1]$. SRC is the relative change $\Delta Y / \sigma_Y$ of Y due to the relative change $\Delta X_i / \sigma_{X_i}$ of the parameter X_i considered (both with respect to their standard deviation σ). Hence, SRC_{*i*} is independent of the units, scale and size of the parameters, and thus sensitivity analysis comes close to an uncertainty analysis. A positive SRC_{*i*} value indicates that increasing a parameter value will cause an increase in the calculated model output, while a negative value indicates a decrease in the output considered caused by a parameter increase.

The sum of squares of SRC_{*i*} values of all parameters equals the coefficient of determination (R^2), which for a perfect fit equals 1. Hence, SRC_{*i*}² / R^2 yields the contribution of parameter X_i to Y . For example, a parameter X_i with SRC_{*i*} = 0.1 adds 0.01 or 1% to Y in case R^2 equals 1.

Coupling global models for hydrology and nutrient loading

A. H. W. Beusen et al.

Title Page

Abstract

Introduction

Conclusions

References

Tables

Figures



Back

Close

Full Screen / Esc

Printer-friendly Version

Interactive Discussion



3 Analysis of the model results

3.1 Comparison with measurement data

We first compared the IMAGE-GNM model results with observed annual (discharge weighed) concentrations for the rivers Rhine, Meuse and Mississippi (see SI1). The model performance for the river Rhine for N concentrations (RMSE = 15 %) is better than for the Meuse and Mississippi (Fig. 6a, b, d, e, g, h). IMAGE-GNM overestimates N concentrations in the river Meuse (RMSE = 31 %) in almost all years; the model underestimates N concentrations in the early 1980s for the Mississippi, while its performance is better from the second half of the 1980s (RMSE for Mississippi = 24 %). P concentrations in the Mississippi are consistently underestimated (RMSE = 51 %) (Fig. 7a, b, d, e, g, h). P concentrations are overestimated in the Rhine in all years with data, although the declining trend is well captured (RMSE = 28 %). The modelled P concentrations are close to observations in the Meuse, with deviations in both directions (RMSE = 36 %).

The residues (observation minus simulation) for the observed versus simulated concentrations of N and P (Figs. 6c and 7c) in the Mississippi show a very clear trend from overestimation at low concentrations to underestimation at high concentrations. The residues show a trend in the Rhine, with a slight increase along with increasing concentrations (Figs. 6f and 7f). The Meuse also shows such trends, although less clear. For P the residue increases with increasing concentration, and for N the opposite occurs (Figs. 6i and 7i).

Since the deviations from observed concentrations can stem from errors in the hydrology, we compared the simulated versus observed discharge (Fig. 8). Results for the Mississippi (Fig. 8a) show a good agreement but with overestimation in most years. While the RMSE is 22 % for the Mississippi, there is no consistent trend between residue and discharge, indicating no systematic error (Fig. 8b). The RMSE for the discharge of the Rhine is 14 %, with a consistent underestimation by the model (Fig. 8c), and the residues show a clear increase with observed discharge (Fig. 8d), indicating a systematic error in the model. For the Meuse, the RMSE for the discharge is 23 %, the

Title Page

Abstract

Introduction

Conclusions

References

Tables

Figures



Back

Close

Full Screen / Esc

Printer-friendly Version

Interactive Discussion



discharge seems to be overestimated (Fig. 8e), and there is only a small trend between discharge and residue (Fig. 8f).

Overall, while discharge is overestimated in the Mississippi, N and P concentrations are underestimated in most years, indicating that part of the problem is in the hydrology.

The hydrology model consistently underestimates discharge, while N concentrations are underestimated in most years, and P is underestimated in the first period up till about 1980, and after this year there is a slight overestimation. So apparently errors in the hydrology can not explain those in the nutrient concentrations. The discharge of the Meuse is overestimated, simulated P concentrations are in good agreement with observations, while N concentrations are overestimated; hence, there is no clear connection between the model errors in discharge and nutrients.

Another performance test involves a direct comparison between aggregated data and model results for a large number of European rivers (see S11) (European Environment Agency, 2013). This dataset includes monitoring data at different stations for 125 rivers, 49 for N and 76 for P. Measurements for some stations were removed from the dataset as outliers (Table S11). Results for all measurements show a coefficient of determination of 0.59 and RMSE of 124 % for N ($n = 709$) and 0.58 and RMSE of 184 % for P ($n = 1010$) (Fig. 9a and b). Results show reasonable coefficients of determination (r^2) of 0.79 and RMSE of 112 % for P and 0.55 and RMSE of 95 % for N (Fig. 9c and d). The average of all measurements for N and P is slightly lower than the simulated concentrations (0.16 versus 0.25 mg PL⁻¹ and 1.25 versus 1.78 mg NL⁻¹). The mean of observations and model values over the monitoring period for each station showed good agreement (Fig. 9e and f). There is also good agreement between model and data for the mean for all stations for each year with deviations never exceeding 1 mg NL⁻¹ and 0.2 mg PL⁻¹ (Fig. 9e and f). It is clear that the model has problems when modelling individual stations in small rivers in the database. The plotted data for all stations in the European rivers (available as separate graphs in the Supplement) show that the model results for the Danube, for example, are in good agreement with

Coupling global models for hydrology and nutrient loading

A. H. W. Beusen et al.

Title Page

Abstract

Introduction

Conclusions

References

Tables

Figures



Back

Close

Full Screen / Esc

Printer-friendly Version

Interactive Discussion



observations for two stations. Most simulated concentrations are within a factor of two of the observed concentrations in the EEA database.

Our model results also show a fair agreement with the validation dataset for the early 1990s for total N collected by Van Drecht et al. (2003) (Fig. 10). Modeled total N concentrations for the Amazon for the early to mid-1980s ($0.7\text{--}0.9\text{ mgL}^{-1}$) are close to measured values ($0.4\text{--}0.5$), and results for total P (0.07 mgL^{-1}) are also close to observations (0.06 mgL^{-1}) (Meybeck and Ragu, 1995; Forsberg et al., 1988).

These comparisons of our model output with data at various aggregation levels show that IMAGE-GNM based on three calibrated submodels (hydrology, nutrient input and in-stream removal) performs very well without any tuning of the overall, integrated model. We have deliberately chosen to not further tune the model so that we can identify its shortcomings. Further improvement of model performance requires a sensitivity analysis.

3.2 Model sensitivity

The influence of a range of parameters on model sensitivity was investigated for modeled N and P delivery, retention and river export. Here we discuss only those parameters that are significant and have an SRC value > 0.2 or < -0.2 (parameters that add $> 4\%$ to the delivery, retention or river export). Results presented in Tables 4 and 5 show that the sensitivity of N delivery, retention and river export for the year 2000 differs from that of P in many aspects.

Total runoff (q_{tot} ; Eq. 5) is significant for retention and river export of both N and P; runoff largely determines all transport pathways and flows of N (runoff, leaching, groundwater flow, and also in-stream retention), and it determines P runoff, the major transport pathway for P. The soil N budget in natural ecosystems and arable land ($N_{\text{budget,crops}}$; $N_{\text{budget,nat}}$; Eq. 1) are important factors for the N delivery, but not for the retention and river export. For P the soil budgets are less important, because soil P content (P_{soil}) and bulk density (B_{soil}) govern the runoff of P more than the budget; actually, soil P content is actually a result of the long-term soil P budget.

Coupling global models for hydrology and nutrient loading

A. H. W. Beusen et al.

Title Page

Abstract

Introduction

Conclusions

References

Tables

Figures



Back

Close

Full Screen / Esc

Printer-friendly Version

Interactive Discussion



Coupling global models for hydrology and nutrient loading

A. H. W. Beusen et al.

Title Page

Abstract

Introduction

Conclusions

References

Tables

Figures



Back

Close

Full Screen / Esc

Printer-friendly Version

Interactive Discussion



stream processes. However, two parts of the model have a dominant importance for the model results, i.e. total runoff from the water balance model PCR-GLOBWB and the factors determining the in-stream biogeochemistry including the uptake velocity and factors used in the parameterization of sub-grid processes for streams and rivers of Strahler orders 6 and less. Here we do not touch upon improvements of the hydrology model and focus on the nutrient-related processes, but see a clear need for improvement of the way the water flow in lakes and reservoirs is simulated, i.e. only the water that actually enters and leaves the lake is considered, with no role for the total water mass. Also, there is a need to improve the geohydrological information in order to better describe global aquifers, their thickness and their denitrification potential.

To improve the in-stream process description a first short-term improvement is to add processes in sediments to allow for simulating P saturation of sediments and desorption in case of decreasing river P loads.

The current model version uses air temperature as a proxy for water temperature. A clear improvement would be to use water temperatures in the spiraling approach, since there may be large differences, especially in low-order streams. Other examples are large rivers influenced by cooling water from nuclear or other power plants. The river Meuse is such an example, and the overestimation of N concentrations may be caused by underestimation of the water temperature.

The importance of factors such as the P content of the soil call for attention to the description of the processes determining P (and N) transport to surface water via surface runoff. Our approach distinguishes an instant transport route, and the transport of soil material with the memory simulated by changing P content of the soil. The delay of the transport may be an important aspect to consider, but at present we have no data available to do so.

Longer term improvements center on the incorporation of a mechanistic model for describing biogeochemical processes in the water column and sediment. This allows further analysis of individual processes and their interplay (plant uptake, sedimentation, benthic processes, denitrification). This will involve a change to a temporal resolu-

hydrological measures or climate-induced changes on nutrient processing and export and therefore on the functioning of downstream ecosystems.

Moreover, GNM is fully integrated into the integrated assessment model IMAGE and can thus provide nutrient transport and processing estimates fully consistent with scenarios based on, for example, the story lines of the shared socioeconomic pathways currently in use by the global climate change community (Kriegler et al., 2014).

An interesting application of IMAGE-GNC is to study the impacts of increasing river export, i.e. eutrophication of coastal marine ecosystems leading to phenomena such as increased production and hypoxia. The changing nutrient stoichiometry in freshwater and coastal systems may lead to phenomena such as harmful algal blooms. Such analyses require coupling our model to coastal biogeochemistry models.

The Supplement related to this article is available online at doi:10.5194/gmdd-8-7477-2015-supplement.

Author contributions. A. H. W. Beusen and A. F. Bouwman developed the model for the delivery of nutrients to surface water on the basis of the work presented in Van Drecht et al. (2003). A. H. W. Beusen, J. M. Mogollón and L. P. H. Van Beek integrated IMAGE-GNM and PCR-GLOBWB and further developed the routing, J. J. Middelburg, J. M. Mogollón, A. F. Bouwman and L. P. H. Van Beek wrote the text.

Acknowledgements. This paper was supported by the Water, Climate and Ecosystems project, part of the Sustainability strategic theme of Utrecht University (<http://wce.uu.nl/>), and contributes to the Netherlands Earth System Science Centre (NESSC, <http://www.nessc.nl/>). We gratefully acknowledge financial support from the Global Environment Facility (GEF), United Nations Environment Programme (UNEP), Intergovernmental Oceanographic Commission of the UNESCO (IOC/UNESCO) and other partners through the UNEP/GEF project “Global Foundations for Reducing Nutrient Enrichment and Oxygen Depletion from Land-based Pollution in Support of Global Nutrient Cycle” (GNC project). Additional funding was provided by the EU H2020 (MSCA award 661163).

Coupling global models for hydrology and nutrient loading

A. H. W. Beusen et al.

Title Page

Abstract

Introduction

Conclusions

References

Tables

Figures



Back

Close

Full Screen / Esc

Printer-friendly Version

Interactive Discussion



References

- Adam, J. C. and Lettenmaier, D. P.: Application of new precipitation and reconstructed streamflow products to streamflow trend attribution in Northern Eurasia, *J. Climate*, 21, 1807–1828, 2008.
- 5 Alcamo, J., Döll, P., Henrichs, T., Kaspar, F., Lehner, B., Rösch, T., and Siebert, S.: Development and testing the WaterGAP 2 model of water use and availability, *Hydrol. Sci.*, 48, 317–337, 2003.
- Alexander, R. B., Smith, R. A., Schwarz, G. E., Boyer, E. W., Nolan, J. V., and Brakebill, J. W.: Differences in phosphorus and nitrogen delivery to the Gulf of Mexico from the Mississippi river basin, *Environ. Sci. Technol.*, 42, 822–830, 2008.
- 10 Allen, R. G., Pereira, L. S., Raes, D., and Smith, M.: Crop evapotranspiration – guidelines for computing crop water requirements, Food and Agriculture Organization of the United Nations, Rome, FAO Irrigation and Drainage Paper 56, available at: www.fao.org/docrep/X0490E/X0490E00.htm (last access: 31 August 2015), 1998.
- 15 Angel, S., Sheppard, S., and Civco, D.: The dynamics of global urban expansion, The World Bank, Transport and Urban Development Department, available at: http://siteresources.worldbank.org/INTURBANDEVELOPMENT/Resources/dynamics_urban_expansion.pdf (last access: 31 August 2015), Washington, D.C., 2005.
- Batjes, N. H.: Total carbon and nitrogen in the soils of the world, *European J. Soil Sci.*, 47, 151–163, 1996.
- 20 Batjes, N. H.: A world dataset of derived soil properties by FAO-UNESCO soil unit for global modelling, *Soil Use Manage.*, 13, 9–16, 1997.
- Batjes, N. H.: Revised soil parameter estimates for the soil types of the world, *Soil Use Manage.*, 18, 232–235, 2002.
- 25 Beusen, A. H. W., Slomp, C. P., and Bouwman, A. F.: Global land–ocean linkage: Direct inputs of nitrogen to coastal waters via submarine groundwater discharge, *Environ. Res. Lett.*, 8, 034035, doi:10.1088/1748-9326/8/3/034035, 2013.
- Bogena, H., Kunkel, R., Schobel, T., Schrey, H. P., and Wendland, F.: Distributed modeling of groundwater recharge at the macroscale, *Ecol. Model.*, 187, 15–26, 2005.
- 30 Böhlke, J.-K., Wanty, R., Tuttle, M., Delin, G., and Landon, M.: Denitrification in the recharge area and discharge area of a transient agricultural nitrate plume in a glacial outwash sand

GMDD

8, 7477–7539, 2015

Coupling global models for hydrology and nutrient loading

A. H. W. Beusen et al.

Title Page

Abstract

Introduction

Conclusions

References

Tables

Figures



Back

Close

Full Screen / Esc

Printer-friendly Version

Interactive Discussion



Coupling global models for hydrology and nutrient loading

A. H. W. Beusen et al.

Title Page

Abstract

Introduction

Conclusions

References

Tables

Figures



Back

Close

Full Screen / Esc

Printer-friendly Version

Interactive Discussion



aquifer, Minnesota, *Water Resour. Res.*, 38, 10-11–10-26, doi:10.1029/2001WR000663, 2002.

Borah, D. K. and Bera, M.: Watershed-scale hydrologic and nonpoint-source pollution models: Review of mathematical bases, *T. Am. Soc. Agric. Eng.*, 46, 1553–1566, 2003.

Bouwman, A. F., Fung, I., Matthews, E., and John, J.: Global analysis of the potential for N₂O production in natural soils, *Global Biogeochem. Cycles*, 7, 557–597, 1993.

Bouwman, A. F., Pawłowski, M., Liu, C., Beusen, A. H. W., Shumway, S. E., Glibert, P. M., and Overbeek, C. C.: Global hindcasts and future projections of coastal nitrogen and phosphorus loads due to shellfish and seaweed aquaculture, *Rev. Fish. Sci.*, 19, 331–357, doi:10.1080/10641262.2011.603849, 2011.

Bouwman, A. F., Beusen, A. H. W., Griffioen, J., Van Groenigen, J. W., Heffting, M. M., Oenema, O., Van Puijenbroek, P. J. T. M., Seitzinger, S., Slomp, C. P., and Stehfest, E.: Global trends and uncertainties in terrestrial denitrification and N₂O emissions, *Phil. T. Roy. Soc. B: Biological Sciences*, 368, 1621, doi:10.1098/rstb.2013.0112, 2013a.

Bouwman, A. F., Beusen, A. H. W., Overbeek, C. C., Bureau, D. P., Pawłowski, M., and Glibert, P. M.: Hindcasts and future projections of global inland and coastal nitrogen and phosphorus loads due to finfish aquaculture, *Rev. Fish. Sci.*, 21, 112–156, doi:10.1080/10641262.2013.790340, 2013b.

Bouwman, A. F., Bierkens, M. F. P., Griffioen, J., Heffting, M. M., Middelburg, J. J., Middelkoop, H., and Slomp, C. P.: Nutrient dynamics, transfer and retention along the aquatic continuum from land to ocean: towards integration of ecological and biogeochemical models, *Biogeosciences*, 10, 1–22, doi:10.5194/bg-10-1-2013, 2013c.

Bouwman, A. F., Klein Goldewijk, K., Van der Hoek, K. W., Beusen, A. H. W., Van Vuuren, D. P., Willems, W. J., Rufino, M. C., and Stehfest, E.: Exploring global changes in nitrogen and phosphorus cycles in agriculture induced by livestock production over the 1900–2050 period, *Proc. Natl. Acad. Sci. USA*, 110, 20882–20887, doi:10.1073/pnas.1012878108, 2013d.

Brady, N. C.: *The nature and properties of soils*, Macmillan Publishing Company, New York, 1990.

Canadell, J., Jackson, R. B., Ehleringer, J. R., Mooney, H. A., Sala, O. E., and Schulze, E. D.: Maximum rooting depth of vegetation types at the global scale, *Oecologia*, 108, 583–595, 1996.

Cerdan, O., Govers, G., Le Bissonnais, Y., Van Oost, K., Poesen, J., Saby, N., Gobin, A., Vacca, A., Quinton, J., Auerswald, K., Klik, A., Kwaad, F. J. P. M., Raclot, D., Ionita, I., Rejman,

Coupling global models for hydrology and nutrient loading

A. H. W. Beusen et al.

Title Page

Abstract

Introduction

Conclusions

References

Tables

Figures



Back

Close

Full Screen / Esc

Printer-friendly Version

Interactive Discussion



J., Rousseva, S., Muxart, T., Roxo, M. J., and Dostal, T.: Rates and spatial variations of soil erosion in Europe: A study based on erosion plot data, *Geomorphology*, 122, 167–177, doi:10.1016/j.geomorph.2010.06.011, 2010.

Cole, J. J., Prairie, Y. T., Caraco, N. F., McDowell, W. H., Tranvik, L. J., Striegl, R. G., Duarte, C. M., Kortelainen, P., Downing, J. A., Middelburg, J. J., and Melack, J.: Plumbing the global carbon cycle: Integrating inland waters into the terrestrial carbon budget, *Ecosystems*, 10, 172–185, 2007.

Dentener, F., Stevenson, D., Ellingsen, K., Noije, T. v., Schultz, M., Amann, M., Atherton, C., Bell, N., Bergmann, D., Bey, I., Bouwman, L., Butler, T., Cofala, J., Collins, B., Drevet, J., Doherty, R., Eickhout, B., Eskes, H., Fiore, A., Gauss, M., Hauglustaine, D., Horowitz, L., Isaksen, I. S. A., Josse, B., Lawrence, M., Krol, M., Lamarque, J. F., Montanaro, V., Müller, J. F., Peuch, V. H., Pitari, G., Pyle, J., Rast, S., Rodriguez, J., Sanderson, M., Savage, N. H., Shindell, D., Strahan, S., Szopa, S., Sudo, K., Dingenen, R. V., Wild, O., and Zeng, G.: The global atmospheric environment for the next generation, *Environ. Sci. Technol.*, 40, 3586–3594, 2006.

de Wit, M. J. M.: Nutrient fluxes at the river basin scale. I: The PolFlow model, *Hydrol. Processes*, 15, 743–759, 2001.

de Wit, M. and Pebesma, E.: Nutrient fluxes at the river basin scale. II: The balance between data availability and model complexity, *Hydrol. Processes*, 15, 761–775, 2001.

Döll, P. and Lehner, B.: Validation of a new global 30-min drainage direction map, *J. Hydrol.*, 258, 214–231, 2002.

Ducharne, A., Baubion, C., Beaudoin, N., Benoit, M., Billen, G., Brisson, N., Garnier, J., Kieken, H., Lebonvallet, S., Ledoux, E., Mary, B., Mignolet, C., Poux, X., Sauboua, E., Schott, C., They, S., and Viennot, P.: Long term prospective of the Seine river system: Confronting climatic and direct anthropogenic changes, *Sci. Tot. Environ.*, 375, 292–311, 2007.

Dürr, H. H., Meybeck, M., and Dürr, S.: Lithologic composition of the earth's continental surfaces derived from a new digital map emphasizing riverine material transfer, *Global Biogeochem. Cycles*, 19, GB4S10, doi:10.1029/2005GB002515, 2005.

European Environment Agency (EEA): Nitrate concentrations in groundwater between 1992 and 2010 in different geographical regions of Europe, available at: <http://www.Eea.Europa.Eu/data-and-maps/figures/nitrate-concentrations-in-groundwater-between-1992-and-2005-in-different-regions-of-europe-3>, last access: 6 January 2013.

Coupling global models for hydrology and nutrient loading

A. H. W. Beusen et al.

Title Page

Abstract

Introduction

Conclusions

References

Tables

Figures



Back

Close

Full Screen / Esc

Printer-friendly Version

Interactive Discussion



- European Environment Agency (EEA): Waterbase rivers version 13, available at: <http://www.Eea.Europa.Eu/data-and-maps/data/waterbase-rivers-9>, last access: 13 October 2013.
- FAO: The digitized soil map of the world (release 1.0), Food and Agriculture Organization of the United Nations, Rome, World Soil Resources Report 67/1, 1991.
- 5 FAO: Fishstatj – software for fishery statistical time series, available at: <http://www.Fao.Org/fishery/statistics/software/fishstatj/en> (release data March 2013), Fisheries and Aquaculture Information and Statistics Service, Food and Agriculture Organization of the United Nations, Rome, 2013.
- 10 FAO/Unesco: Soil map of the world. Revised legend, FAO, Rome, Italy, World Resources Report 60, 1988.
- Fekete, B. M., Wisser, D., Kroeze, C., Mayorga, E., Bouwman, A. F., Wollheim, W. M., and Vörösmarty, C. J.: Millennium ecosystem assessment scenario drivers (1970–2050): Climate and hydrological alterations, *Global Biogeochem. Cycles*, 24, GB0A12, doi:10.1029/2009GB003593, 2011.
- 15 Firestone, M. K.: Biological denitrification, in: Nitrogen in agricultural soils, edited by: Stevenson, F. J., American Society of Agronomy, Crop Science Society of America, Soil Science Society of America, Madison, Wisconsin, 280–326, 1982.
- Foppen, J. W. A.: Impact of high-strength wastewater infiltration on groundwater quality and drinking water supply: The case of Sana’á, Yemen, *J. Hydrol.*, 263, 198–216, 2002.
- 20 Forsberg, B. R., Devol, A. H., Richey, J. E., Martinelli, L. A., and Dos Santos, H.: Factors controlling nutrient concentrations in Amazon floodplain lakes, *Limnol. Oceanogr.*, 33, 41–56, 1988.
- Green, C. T., Puckett, L. J., Bohlke, J. K., Bekins, B. A., Phillips, S. P., Kaufman, L. J., Denver, J. M., and Johnson, H. M.: Limited occurrence of denitrification in four shallow aquifers in agricultural areas in the United States, *J. Environ. Qual.*, 37, 994–1009, doi:10.1010.2134/jeq2006.0419, 2008.
- 25 Guo, L. B. and Gifford, R. M.: Soil carbon stocks and land use change: A meta analysis, *Global Change Biol.*, 8, 345–360, doi:10.1046/j.1354-1013.2002.00486.x, 2002.
- Haddeland, I., Skaugen, T., and Lettenmaier, D. P.: Anthropogenic impacts on continental surface water fluxes, *Geophys. Res. Lett.*, 33, 8, doi:10.1029/2006GL026047, 2006.
- 30 Hageman, S. and Gates, L. D.: Improving a sub-grid runoff parameterization scheme for climate models by the use of high-resolution data derived from satellite observations, *Clim. Dynam.*, 21, 349–359, 2003.

Coupling global models for hydrology and nutrient loading

A. H. W. Beusen et al.

Title Page

Abstract

Introduction

Conclusions

References

Tables

Figures



Back

Close

Full Screen / Esc

Printer-friendly Version

Interactive Discussion



Hagemann, S., Botzet, M., Dümenil, L., and Machenhauer, B.: Derivation of global GCM boundary conditions from 1 km land use satellite data. Rep. 289, Max Planck Institute for Meteorology, Hamburg, Germany, 1999.

Hart, M. R., Quin, B. F., and Nguyen, M. L.: Phosphorus runoff from agricultural land and direct fertilizer effects: A review, *J. Environ. Qual.*, 33, 1954–1972, 2004.

Hartmann, J., Moosdorf, N., Lauerwald, R., Hinderer, M., and West, A. J.: Global chemical weathering and associated P-release – the role of lithology, temperature and soil properties, *Chem. Geology*, 363, 145–163, doi:10.1016/j.chemgeo.2013.10.025, 2014.

Holdridge, L. R.: Life zone ecology, Tropical Science Center, San Jose, Costa Rica, 206 p., 1967.

Keuskamp, J. A., Van Drecht, G., and Bouwman, A. F.: European-scale modelling of groundwater denitrification and associated N₂O production, *Environ. Pollut.*, 165, 67–76, doi:10.1016/j.envpol.2012.02.008, 2012.

Klein Goldewijk, K., Beusen, A., Van Drecht, G., and De Vos, M.: The HYDE 3.1 spatially explicit database of human induced land use change over the past 12 000 years, *Global Ecol. Biogeography*, 20, 73–86, doi:10.1111/j.1466-8238.2010.00587.x, 2010.

Knowles, R.: Denitrification, *Microb. Rev.*, 46, 43–70, 1982.

Kragt, J. F., De Vries, W., and Breeuwsma, A.: Modelling nitrate leaching on a regional scale, in: *Fertilization and the environment*, edited by: Merckx, R. H., Vereecken, H., and Vlassak, K., Leuven University Press, Leuven, Belgium, 340–347, 1990.

Kriegler, E., Edmonds, J., Hallegatte, S., Ebi, K. L., Kram, T., Riahi, K., Winkler, H., and Van Vuuren, D. P.: A new scenario framework for climate change research: The concept of shared climate policy assumptions, *Clim. Change*, 122, 401–414, 2014.

Lehner, B. and Döll, P.: Development and validation of a global database of lakes, reservoirs and wetlands, *J. Hydrol.*, 296, 1–22, 2004.

Lehner, B., Liermann, C. R., Revenga, C., Vörösmarty, C., Fekete, B., Crouzet, P., Döll, P., Endejan, M., Frenken, K., Magome, J., Nilsson, C., Robertson, J. C., Rödel, R., Sindorf, N., and Wisser, D.: High-resolution mapping of the world's reservoirs and dams for sustainable river-flow management, *Front. Ecol. Environ.*, 9, 494–502, doi:10.1890/100125, 2011.

Marcé, R. and Armengol, J.: Modeling nutrient in-stream processes at the watershed scale using Nutrient Spiralling metrics, *Hydrol. Earth Syst. Sci.*, 13, 953–967, doi:10.5194/hess-13-953-2009, 2009.

Coupling global models for hydrology and nutrient loading

A. H. W. Beusen et al.

Title Page

Abstract

Introduction

Conclusions

References

Tables

Figures



Back

Close

Full Screen / Esc

Printer-friendly Version

Interactive Discussion



Mayorga, E., Seitzinger, S. P., Harrison, J. A., Dumont, E., Beusen, A. H. W., Bouwman, A. F., Fekete, B. M., Kroeze, C., and Van Drecht, G.: Global nutrient export from watersheds 2 (NEWS 2): Model development and implementation, *Environ. Model. Softw.*, 25, 837–853, 2010.

5 McDowell, R. W. and Sharpley, A. N.: Approximating phosphorus release from soils to surface runoff and subsurface drainage, *J. Environ. Qual.*, 30, 508–520, 2001.

McLaughlan, K.: The nature and longevity of agricultural impacts on soil carbon and nutrients: A review, *Ecosystems*, 9, 1364–1382, 2006.

10 Meinardi, C. R.: Groundwater recharge and travel times in the sandy regions of the Netherlands, National Institute for Public Health and the Environment, the Netherlands, Bilthoven, Report 715501004, 1994.

Meybeck, M. and Ragu, A.: River discharges to oceans: An assessment of suspended solids, major ions and nutrients, United Nations Environment Programme (UNEP), 245, 1995.

15 Morée, A. L., Beusen, A. H. W., Bouwman, A. F., and Willems, W. J.: Exploring global nitrogen and phosphorus flows in urban wastes during the twentieth century, *Global Biogeochem. Cycles*, 27, 1–11, doi:10.1002/gbc.20072, 2013.

20 Mulholland, P. J., Helton, A. M., Poole, G. C., Hall, R. O., Hamilton, S. K., Peterson, B. J., Tank, J. L., Ashkenas, L. R., Cooper, L. W., Dahm, C. N., Dodds, W. K., Findlay, S. E. G., Gregory, S. V., Grimm, N. B., Johnson, S. L., McDowell, W. H., Meyer, J. L., Valett, H. M., Webster, J. R., Arango, C. P., Beaulieu, J. J., Bernot, M. J., Burgin, A. J., Crenshaw, C. L., Johnson, L. T., Niederlehner, B. R., O'Brien, J. M., Potter, J. D., Sheibley, R. W., Sobota, D. J., and Thomas, S. M.: Stream denitrification across biomes and its response to anthropogenic nitrate loading, *Nature*, 452, 202–205, 2008.

25 New, M., Hulme, M., and Jones, P.: Representing twentieth-century space-time climate variability. Part II: Development of 1901–96 monthly grids of terrestrial surface climate, *J. Climate*, 13, 2217–2238, 2000.

Newbold, J. D., Elwood, J. W., O'Neill, R. V., and Winkle, W. V.: Measuring nutrient spiraling in streams, *Can. J. Fish. Aquatic Sci.*, 38, 860–863, 1981.

30 Nyenje, P. M., Foppen, J. W., Uhlenbrook, S., Kulabako, R., and Muwanga, A.: Eutrophication and nutrient release in urban areas of sub-Saharan Africa – a review, *Sci. Tot. Environ.*, 408, 447–455, doi:10.1016/j.scitotenv.2009.10.020, 2010.

Peterjohn, W. T. and Schlesinger, W. H.: Nitrogen loss from deserts in the southwestern United States, *Biogeochemistry*, 10, 67–79, 1990.

Coupling global models for hydrology and nutrient loadingA. H. W. Beusen et al.

[Title Page](#)[Abstract](#)[Introduction](#)[Conclusions](#)[References](#)[Tables](#)[Figures](#)[Back](#)[Close](#)[Full Screen / Esc](#)[Printer-friendly Version](#)[Interactive Discussion](#)

- Reddy, K. R., Kadlec, R. H., Flaig, E., and Gale, P. M.: Phosphorus retention in streams and wetlands: A review, *Crit. Rev. Environ. Sci. Technol.*, 29, 83–146, 1999.
- Saltelli, A., Chan, K., and Scott, E. M.: Sensitivity analysis, Wiley and Sons, Chichester, 2000.
- Saltelli, A., Tarantola, S., Campolongo, F., and Ratto, M.: Sensitivity analysis in practice. A guide to assessing scientific models, Wiley and Sons, Chichester, 2004.
- 5 Saunders, D. L. and Kalff, J.: Nitrogen retention in wetlands, lakes and rivers, *Hydrobiologia*, 443, 205–212, doi:10.1023/a:1017506914063, 2001.
- Seitzinger, S. P., Harrison, J. A., Dumont, E., Beusen, A. H. W., and Bouwman, A. F.: Sources and delivery of carbon, nitrogen, and phosphorus to the coastal zone: An overview of global news models and their application, *Global Biogeochem. Cycles*, 19, GB4S01, doi:10.1029/2005GB002606, 2005.
- 10 Seitzinger, S. P., Mayorga, E., Bouwman, A. F., Kroeze, C., Beusen, A. H. W., Billen, G., Van Drecht, G., Dumont, E., Fekete, B. M., Garnier, J., Harrison, J., Wisser, D., and Wollheim, W. M.: Global river nutrient export: A scenario analysis of past and future trends, *Global Biogeochem. Cycles*, 24, GB0A08, doi:10.1029/2009GB003587, 2010.
- Shaffer, M. J., Halvorson, A. D., and Pierce, F. J.: Nitrate leaching and economic analysis package (NLEAP): Model description and application, in: *Managing nitrogen for groundwater quality and farm profitability*, edited by: Follet, R. F., Keeney, D. R., and Cruse, R. M., Soil Sci. Soc. America, Madison, Wisconsin, USA, 285–322, 1991.
- 20 Shand, P. and Edmunds, W. M.: The baseline inorganic chemistry of European groundwater, in: *Natural groundwater quality*, edited by: Edmunds, W. M. and Shand, P., Blackwell, Oxford, 22–58, 2008.
- Simek, M. and Cooper, J. E.: The influence of soil pH on denitrification: Progress towards the understanding of this interaction over the last 50 years, *European J. Soil Sci.*, 53, 345–354, 2002.
- 25 Smith, R. A., Schwarz, G. E., and Alexander, R. B.: Regional interpretation of water-quality monitoring data, *Water Resour. Res.*, 33 2781–2798, 1997.
- Stanley, E. H., Powers, S. M., and Lottig, N. R.: The evolving legacy of disturbance in stream ecology: Concepts, contributions, and coming challenges, *J. North American Benthol. Soc.*, 29, 67–83, doi:10.1899/08-027.1, 2010.
- 30 Stehfest, E., Van Vuuren, D. P., Kram, T., and Bouwman, A. F.: Integrated assessment of global environmental change with IMAGE 3.0. Model description and policy applications,

Coupling global models for hydrology and nutrient loading

A. H. W. Beusen et al.

Title Page

Abstract

Introduction

Conclusions

References

Tables

Figures



Back

Close

Full Screen / Esc

Printer-friendly Version

Interactive Discussion



in: PBL Netherlands Environmental Assessment Agency, available at: http://themasites.pbl.nl/models/image/index.php/Main_Page (last access: 14 May 2015), The Hague, 2014.

Strahler, A. N.: Quantitative analysis of watershed geomorphology, *T. American Geophysical Union*, 38, 913–920, 1957.

5 Tarkalson, D. D. and Mikkelsen, R. L.: Runoff phosphorus losses as related to soil test phosphorus and degree of phosphorus saturation on piedmont soils under conventional and no-tillage, *Communications Soil Sci. Plant Anal.*, 35, 2987–3007, 2004.

Todini, E.: The ARNO rainfall-runoff model, *J. Hydrol.*, 175, 339–382, 1996.

10 Trumbore, S. E., Davidson, E. A., Camarge, P. B. D., Nepstad, D. C., and Martinelli, L. A.: Below-ground cycling of carbon in forests and pastures of eastern Amazonia, *Global Biogeochem. Cycles*, 9, 515–528, 1995.

Uppala, S. M., Kållberg, P. W., Simmons, A. J., Andrae, U., da Costa Bechtold, V., Fiorino, M., Gibson, J. K., Haseler, J., Hernandez, A., Kelly, G. A., Li, X., Onogi, K., Saarinen, S., Sokka, N., Allan, R. P., Andersson, E., Arpe, K., Balmaseda, M. A., Beljaars, A. C. M., Van De Berg, L., Bidlot, J., Bormann, N., Caires, S., Chevallier, F., Dethof, A., Dragosavac, M., Fisher, M., Fuentes, M., Hagemann, S., Hólm, E., Hoskins, B. J., Isaksen, L., Janssen, P. A. E. M., Jenne, R., McNally, A. P., Mahfouf, J. F., Morcrette, J. J., Rayner, N. A., Saunders, R. W., Simon, P., Sterl, A., Trenberth, K. E., Untch, A., Vasiljevic, D., Viterbo, P., and Woollen, J.: The ERA-40 re-analysis, *Q. J. Roy. Meteorol. Soc.*, 131, 2961–3012, 2005.

20 Van Beek, L. P. H., Wada, Y., and Bierkens, M. F. P.: Global monthly water stress: 1. Water balance and water availability, *Water Resour. Res.*, 47, W07517, doi:10.1029/2010wr009791, 2011.

Van Cleemput, O.: Subsoils: Chemo- and biological denitrification, N_2O and N_2 emissions, *Nut. Cycling Agroecosyst.*, 52, 187–194, 1998.

25 Van den Brink, C., Frapporti, G., Griffioen, J., and Zaadnoordijk, W. J.: Statistical analysis of anthropogenic versus geochemical-controlled differences in groundwater composition in the netherlands, *J. Hydrol.*, 336, 470–480, 2007.

Van Den Heuvel, R. N., Van Den Biezen, E., Jetten, M. S. M., Hefting, M. M., and Kartal, B.: Denitrification at pH 4 by a soil-derived Rhodanobacter-dominated community, *Environ. Microbiol.*, 12, 3264–3271, 2010.

30 Van Den Heuvel, R. N., Bakker, S. E., Jetten, M. S. M., and Hefting, M. M.: Decreased N_2O reduction by low soil pH causes high N_2O emissions in a riparian ecosystem, *Geobiology*, 9, 294–300, 2011.

Coupling global models for hydrology and nutrient loading

A. H. W. Beusen et al.

Title Page

Abstract

Introduction

Conclusions

References

Tables

Figures



Back

Close

Full Screen / Esc

Printer-friendly Version

Interactive Discussion



- Van Drecht, G., Bouwman, A. F., Knoop, J. M., Beusen, A. H. W., and Meinardi, C. R.: Global modeling of the fate of nitrogen from point and nonpoint sources in soils, groundwater and surface water, *Global Biogeochem. Cycles*, 17, 1115, doi:10.1029/2003GB002060, 2003.
- Van Drecht, G., Bouwman, A. F., Boyer, E. W., Green, P., and Siebert, S.: A comparison of global spatial distributions of nitrogen inputs for nonpoint sources and effects on river nitrogen export, *Global Biogeochem. Cycles*, 19, GB4S06, doi:10.1029/2005GB002454, 2005.
- Velthof, G. L., Oudendag, D. A., and Oenema, O.: Development and application of the integrated nitrogen model MITERRA-EUROPE, Alterra, Wageningen UR, the Netherlands; EuroCare, University of Bonn, Germany, ASG, Wageningen UR, the Netherlands, Wageningen, 102, 2007.
- Velthof, G. L., Oudendag, D., Witzke, H. P., Asman, W. A. H., Klimont, Z., and Oenema, O.: Integrated assessment of nitrogen losses from agriculture in EU-27 using MITERRA-EUROPE, *J. Environ. Qual.*, 38, 402–417, 2009.
- Verdin, K. L. and Greenlee, S. K.: Development of continental scale digital elevation models and extraction of hydrographic features. Paper presented at third international conference/workshop on integrating GIS and environmental modeling. National center for geographical information and analysis, Santa Barbara, California, 1996.
- Vidon, P. G. and Hill, A. R.: A landscape-based approach to estimate riparian hydrological and nitrate removal functions, *J. Am. Water Resour. Assoc.*, August 2006, 1099–1112, 2006.
- Vitousek, P. M.: Litterfall, nutrient cycling, and nutrient limitation in tropical forests, *Ecology*, 65, 285–298, 1984.
- Vitousek, P. M., Fahey, T., Johnson, D. W., and Swift, M. J.: Element interactions in forest ecosystems: Succession, allometry and input–output budgets, *Biogeochemistry*, 5, 7–34, 1988.
- Vogt, K. A., Grier, C. C., and Vogt, D. J.: Production, turnover, and nutrient dynamics of above- and belowground detritus of world forests, *Adv. Ecol. Res.*, 15, 303–377, 1986.
- Wakida, F. T. and Lerner, D. N.: Non agricultural sources of groundwater nitrate: A review and a case study, *Water Resour.*, 39, 3–16, 2005.
- Walvoord, M. A., Phillips, F. M., Stonestrom, D. A., Evans, R. D., Hartsough, P. C., Newman, B. D., and Striegl, R. G.: A reservoir of nitrate beneath desert soils, *Science*, 302, 1021–1024, 2003.

- Wollheim, W. M., Vörösmarty, C. J., Peterson, B. J., Seitzinger, S. P., and Hopkinson, C. S.: Relationship between river size and nutrient removal, *Geophys. Res. Lett.*, 33, 6, doi:10.1029/2006GL025845, 2006.
- 5 Wollheim, W. M., Peterson, B. J., Thomas, S. M., Hopkinson, C. H., and Vörösmarty, C. J.: Dynamics of N removal over annual time periods in a suburban river network, *J. Geophys. Res.*, 113, G3, doi:10.1029/2007JG000660, 2008a.
- 10 Wollheim, W., Vörösmarty, C. J., Bouwman, A. F., Green, P., Harrison, J., Meybeck, M., Peterson, B. J., Seitzinger, S. P., and Syvitski, J.: Global N removal by freshwater aquatic systems using a spatially distributed, within-basin approach, *Global Biogeochem. Cycles*, 22, GB2026, doi:10.1029/2007GB002963, 2008b.
- Yang, X., Post, W. M., Thornton, P. E., and Jain, A.: The distribution of soil phosphorus for global biogeochemical modeling, *Biogeosciences*, 10, 2525–2537, doi:10.5194/bg-10-2525-2013, 2013.

Coupling global models for hydrology and nutrient loadingA. H. W. Beusen et al.

[Title Page](#)[Abstract](#)[Introduction](#)[Conclusions](#)[References](#)[Tables](#)[Figures](#)[Back](#)[Close](#)[Full Screen / Esc](#)[Printer-friendly Version](#)[Interactive Discussion](#)

Table 3. Model parameters included in the sensitivity analysis, their symbol and description, for which nutrient it is used, and the standard, minimum, mode and maximum value considered for the sampling procedure. Parameters are listed in alphabetical order of their symbol.

Symbol	Description	Nutrient	Distribution ^a	Standard	Min.	Max.
A	Width factor	N/P	U3	8.3	7.5	9.1
A_1	Drainage area first order stream	N/P	U3	2.6	2.3	2.9
A_{flooding}	Area of flooding areas	N/P	U1	1.0	0.9	1.1
B	Width exponent	N/P	U3	0.52	0.47	0.57
B_{soil}	Bulk density of the soil	N/P	U1	1.0	0.9	1.1
CN_{gnpp}	CN weight ratio of gnpp in flooding areas	N	U3	100	90	110
$CN_{\text{soil,crop}}$	CN weight ratio of soil loss under crops	N	U3	12	11	13
$CN_{\text{soil,grass}}$	CN weight ratio of soil loss under grassland	N	U3	14	12.5	15.5
$CN_{\text{soil,nat}}$	CN weight ratio of soil loss under natural ecosystems	N	U3	14	12.5	15.5
CP_{aomi}	CP weight ratio of gnpp in flooding areas	P	U3	1200	1080	1320
$C_{\text{sro,N}}$	Correction coefficient for N in surface runoff	N	U3	0.3	0.27	0.33
$C_{\text{sro,P}}$	Correction constant for P in surface runoff	P	U3	0.3	0.27	0.33
D_{dgrw}	Thickness of deep groundwater system	N	U3	50.0	45	55
D_{flooding}	Depth of flooding areas	N/P	U1	1.0	0.9	1.1
D_{rip}	Thickness of riparian zone	N	U3	0.3	0.27	0.33
D_{sgrw}	Thickness of shallow groundwater system	N	U3	5.0	4.5	5.5
$dt50_{\text{den,dgrw}}$	Half-life of nitrate in deep groundwater	N	U3	∞	50.0	100.0
$dt50_{\text{den,sgrw}}$	Half-life of nitrate in shallow groundwater	N	U1	1.0	0.9	1.1
F_{aomi}	Reduction factor for litter load to surface water	N/P	U1	0.5	0.45	0.55
$F_{\text{leach,crop}}$	Reduction fraction of N towards the shallow groundwater system	N	U3	1.0	0.9	1.0
$F_{\text{leach,grass}}$	Reduction fraction of N towards the shallow groundwater system	N	U3	0.36	0.32	0.4
$F_{\text{leach,nat}}$	Reduction fraction of N towards the shallow groundwater system	N	U3	0.36	0.32	0.4
f_{qgw}	Fraction of q_{eff} that flows towards the deep system	N	U1	1.0	0.9	1.1
f_{qsr}	Overall runoff fraction	N/P	U1	1.0	0.9	1.1
$f_{\text{qsr}}(\text{crops})$	Land-use effect on surface runoff for soils under crops	N/P	T2	1.0	0.75	1.0
$f_{\text{qsr}}(\text{grass})$	Land-use effect on surface runoff for soils under grassland	N/P	T1	0.25	0.125	0.5
$f_{\text{qsr}}(\text{nat})$	Land-use effect on surface runoff for soils in natural ecosystems	N/P	T3	0.125	0.1	0.3
AOMI	Litterfall in flooding areas	N/P	U1	1.0	0.9	1.1
L_1	Mean length first order stream	N/P	U3	1.6	1.4	1.8
N_{aqua}	N load from aquaculture	N	U1	1.0	0.9	1.1
$N_{\text{budget,crops}}$	N budgets in croplands	N	U1	1.0	0.9	1.1
$N_{\text{budget,grass}}$	N budget in grasslands	N	U1	1.0	0.9	1.1

Coupling global models for hydrology and nutrient loading

A. H. W. Beusen et al.

Title Page

Abstract

Introduction

Conclusions

References

Tables

Figures

◀

▶

◀

▶

Back

Close

Full Screen / Esc

Printer-friendly Version

Interactive Discussion



Table 3. Continued.

Symbol	Description	Nutrient	Distribution ^a	Standard	Min.	Max.
$N_{\text{budget,nat}}$	N budget in natural ecosystems	N	U1	1.0	0.9	1.1
$N_{\text{conc,high}}$	Retention multiplier for retention at high N concentrations.	N	U3	0.3	0.2	0.4
$N_{\text{conc,low}}$	Retention multiplier for retention at low N concentrations.	N	U3	7	6	9
N_{depo}	N deposition on surface water	N	U1	1.0	0.9	1.1
N_{point}	N from point sources	N	U1	1.0	0.9	1.1
$N_{\text{uptake,crops}}$	N uptake in croplands	N	U1	1.0	0.9	1.1
$N_{\text{uptake,grass}}$	N uptake in grasslands	N	U1	1.0	0.9	1.1
P_{aqua}	P load from aquaculture	P	U1	1.0	0.9	1.1
$P_{\text{budget,crops}}$	P budgets in croplands	P	U1	1.0	0.9	1.1
$P_{\text{budget,grass}}$	P budget in grasslands	P	U1	1.0	0.9	1.1
$P_{\text{budget,nat}}$	P budget in natural ecosystems	P	U1	1.0	0.9	1.1
Poros	Porosity of aquifer material	N	U1	1.0	0.9	1.1
P_{point}	P from point sources	P	U1	1.0	0.9	1.1
P_{soil}	P content of the soil	P	U1	1.0	0.9	1.1
$P_{\text{uptake,crops}}$	P uptake in croplands	P	U1	1.0	0.9	1.1
$P_{\text{uptake,grass}}$	P uptake in grasslands	P	U1	1.0	0.9	1.1
$PV_{f,\text{wetland}}$	Net uptake velocity for wetlands	P	U3	44.5	40	49
CP_{Weath}	P content of per lithology class	N	U1	1.0	0.9	1.1
q_{tot}	Runoff (total)	N/P	U1	1.0	0.9	1.1
R_a	Drainage area ratio	N/P	U3	4.7	4.2	5.2
R_b	Stream number ratio	N/P	U3	4.5	4.05	4.95
R_L	Mean length ratio	N/P	U3	2.3	2.0	2.6
Temp	Mean annual air temperature	N/P	U2	0.0	-1.0	1.0
$V_{f,\text{lake}}$	Net uptake velocity for lakes	N	U3	35	32	38
$V_{f,\text{lake}}$	Net uptake velocity for lakes	P	U3	44.5	40	49
$V_{f,\text{reservoir}}$	Net uptake velocity for reservoirs	N	U3	35	32	38
$V_{f,\text{reservoir}}$	Net uptake velocity for reservoirs	P	U3	44.5	40	49
$V_{f,\text{river}}$	Net uptake velocity for rivers	N	U3	35	32	38
$V_{f,\text{river}}$	Net uptake velocity for rivers	P	U3	44.5	40	49
$V_{f,\text{wetland}}$	Net uptake velocity for wetlands	N	U3	35	32	38
V_{water}	Water volume of all water bodies	N/P	U1	1.0	0.9	1.1

^a Samples values are applied to all grid cells. For sampling, either uniform or triangular distributions are used. A triangular distribution is a continuous probability distribution with lower limit a , upper limit b and mode c , where $a \leq c \leq b$. The probability to sample a point depends on the skewness of the triangle. In the case of $d/50_{\text{gen,dgmv}}$, $ac = bc$, and probability to sample a point on the left and right hand side of c is the same. In other cases, for example $f_{Q_{50}}$ (crops) is a fraction [0,1], with standard value of 1.0. To achieve a high probability to sample close to 1.0, the triangle is designed with $b = 1$ and c is close to 1. For some of the above distributions the expected value is not equal to the standard. Since the calculated R^2 for all output parameters exceeds 0.99, this approach for analyzing the sensitivity is still valid. The distributions used are:

- U1. Uniform; values are multipliers for standard values on a grid cell basis.
- U2. Uniform; values are added to the standard values on a grid cell basis.
- U3. Uniform; values are used as such.
- T1. Triangular; values between 0.125 and 0.5 with an expected value of 0.25.
- T2. Triangular; values between 0.75 and 1.0 with an expected value of 0.995.
- T3. Triangular; values between 0.1 and 0.3 with an expected value of 0.125.

Coupling global models for hydrology and nutrient loading

A. H. W. Beusen et al.

Title Page

Abstract Introduction

Conclusions References

Tables Figures

◀ ▶

◀ ▶

Back Close

Full Screen / Esc

Printer-friendly Version

Interactive Discussion



Table 4. Continued.

Parameter	N delivery	N retention	N export
A_{flooding}	0.34	-0.11	0.23
AOMI	0.35	-0.10	0.24
CN_{aomi}	<i>-0.35</i>	0.10	<i>-0.24</i>
F_{aomi}	0.35	-0.10	0.24
A		0.16	-0.12
A_1		-0.04	0.03
B		0.09	-0.07
D_{flooding}		-0.01	0.01
L_1		0.21	-0.16
$N_{\text{conc,high}}$		0.16	-0.12
$N_{\text{conc,low}}$	-0.01	0.40	<i>-0.31</i>
R_a		-0.08	0.06
R_b		0.08	-0.06
R_L		0.53	<i>-0.41</i>
Temp	-0.09	0.41	<i>-0.36</i>
$V_{f,\text{lake,N}}$		0.06	-0.04
$V_{f,\text{reservoir,N}}$		0.07	-0.05
$V_{f,\text{river,N}}$		0.38	<i>-0.30</i>
$V_{f,\text{wetland,N}}$			
V_{water}		0.01	
N_{aqua}	0.03	-0.01	0.02
N_{depo}	0.03	0.01	
N_{point}	0.22	-0.06	0.14

^a Cells with no values represent insignificant SRC values; all cells with values have significant SRC, cells with normal upright font indicate values $-0.2 < \text{SRC} < 0.2$; italic and bold colors indicate values exceeding $+0.2$ and -0.2 , respectively. An SRC value of 0.2 indicates that the parameter concerned has an influence of $0.2^2 = 0.04$ (4%) on the model variable considered.

Coupling global models for hydrology and nutrient loading

A. H. W. Beusen et al.

Title Page

Abstract

Introduction

Conclusions

References

Tables

Figures



Back

Close

Full Screen / Esc

Printer-friendly Version

Interactive Discussion



Coupling global models for hydrology and nutrient loading

A. H. W. Beusen et al.

Title Page

Abstract

Introduction

Conclusions

References

Tables

Figures

◀

▶

◀

▶

Back

Close

Full Screen / Esc

Printer-friendly Version

Interactive Discussion

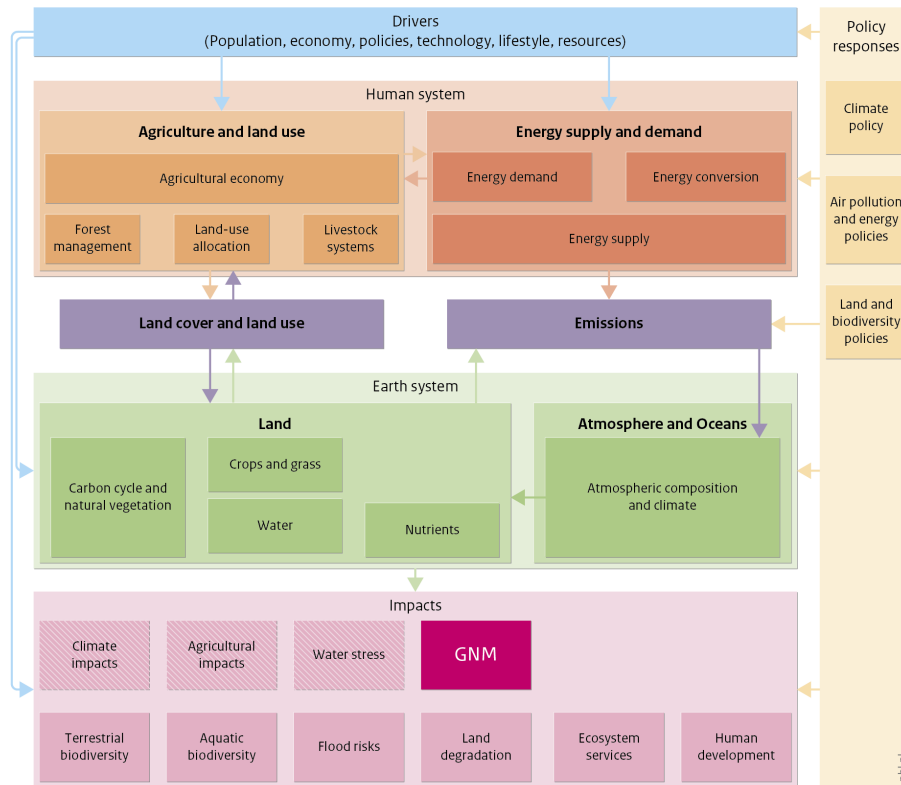


Table 5. Continued.

Parameter	P delivery	P retention	P export
R_L		0.49	-0.38
Temp	0.12	0.27	-0.12
$V_{f, \text{lake}, P}$		0.06	-0.04
$V_{f, \text{reservoir}, P}$		0.10	-0.08
$V_{f, \text{river}, P}$		0.40	-0.30
$V_{f, \text{wetland}, P}$			
V_{water}		0.01	
P_{aqua}	0.01		0.02
P_{point}	0.14	-0.06	0.15

^a See Table 4.

IMAGE 3.0 framework



Source: PBL 2014

Figure 1. Scheme of the Integrated Model to Assess the Global Environment (IMAGE) Modified from Stehfest et al. (2014).

GMDD

8, 7477–7539, 2015

Coupling global models for hydrology and nutrient loading

A. H. W. Beusen et al.

Title Page

Abstract Introduction

Conclusions References

Tables Figures

⏪ ⏩

◀ ▶

Back Close

Full Screen / Esc

Printer-friendly Version

Interactive Discussion



Coupling global models for hydrology and nutrient loading

A. H. W. Beusen et al.

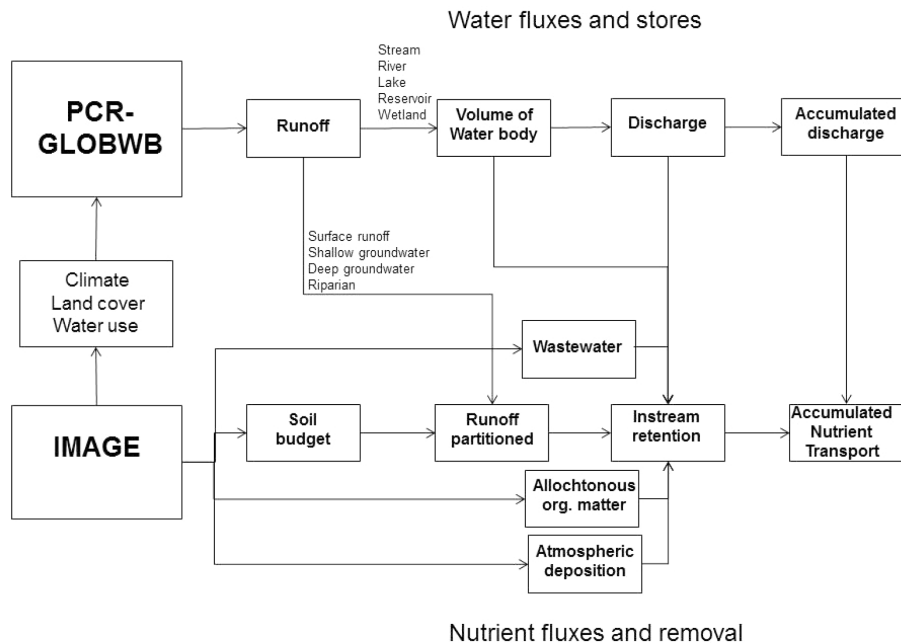


Figure 2. Scheme of the model framework with PCR-GLOBWB and IMAGE and the data flows between the models.

Title Page

Abstract

Introduction

Conclusions

References

Tables

Figures

⏪

⏩

◀

▶

Back

Close

Full Screen / Esc

Printer-friendly Version

Interactive Discussion



Grid cell

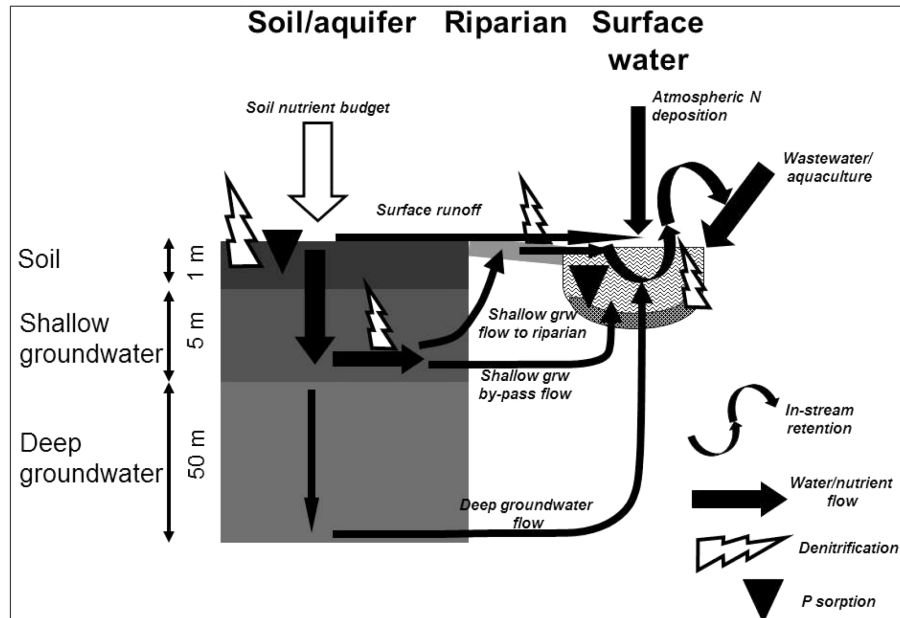


Figure 3. Scheme of the flows of water and nutrients, and retention processes within a grid cell.

[Title Page](#)

[Abstract](#) | [Introduction](#)

[Conclusions](#) | [References](#)

[Tables](#) | [Figures](#)

[◀](#) | [▶](#)

[◀](#) | [▶](#)

[Back](#) | [Close](#)

[Full Screen / Esc](#)

[Printer-friendly Version](#)

[Interactive Discussion](#)



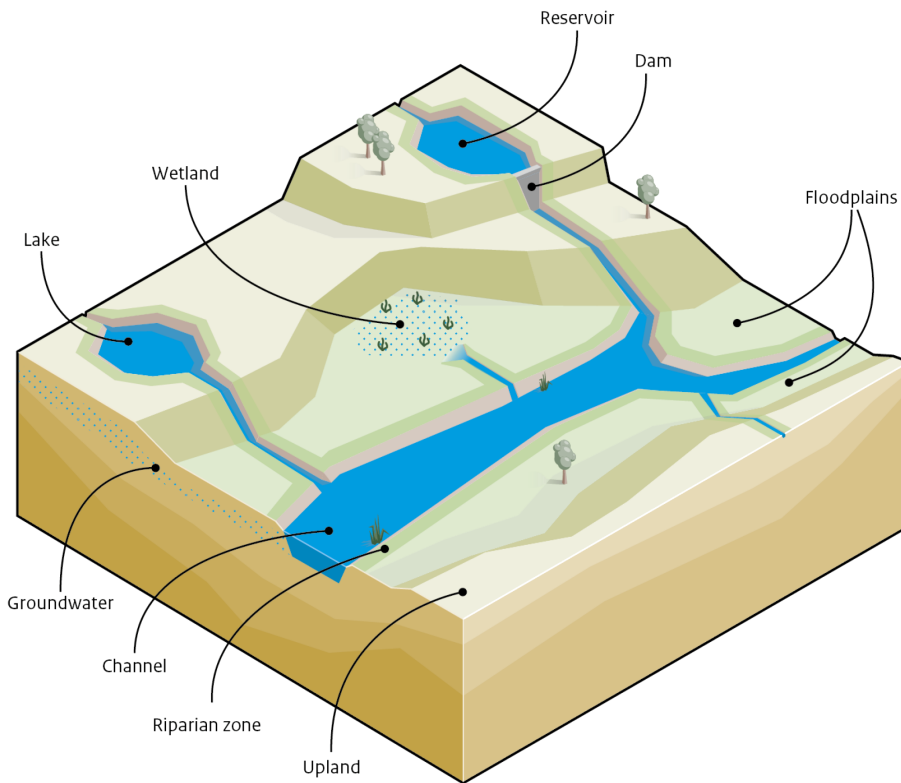


Figure 4. Scheme of the routing of water (with N and P) in a landscape with streams, rivers, lakes, wetlands and reservoirs; each type of water body within a grid cell is defined by an inflow or discharge, depth and area. Floodplains may be temporarily or permanently flooded.

Coupling global models for hydrology and nutrient loading

A. H. W. Beusen et al.

Title Page

Abstract Introduction

Conclusions References

Tables Figures

◀ ▶

◀ ▶

Back Close

Full Screen / Esc

Printer-friendly Version

Interactive Discussion



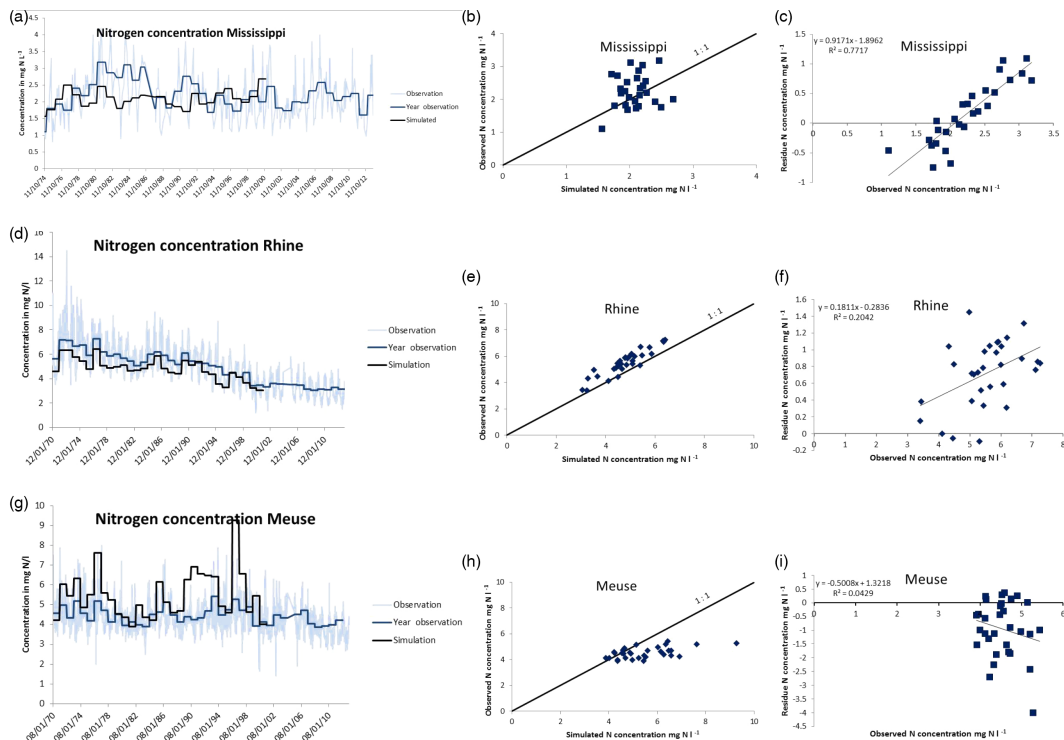


Figure 6. Comparison of modeled (black line) and measured (light blue, and aggregated yearly discharge-weighted concentrations) of total N in the rivers Mississippi (a–c), Rhine (d–f) and Meuse (g–i). Panels on the left are comparisons over time; panels in the center represent plots of simulations versus observations with a 1 : 1 line, and figures on the right are the concentrations versus the residues (observation minus simulation) with a regression line.

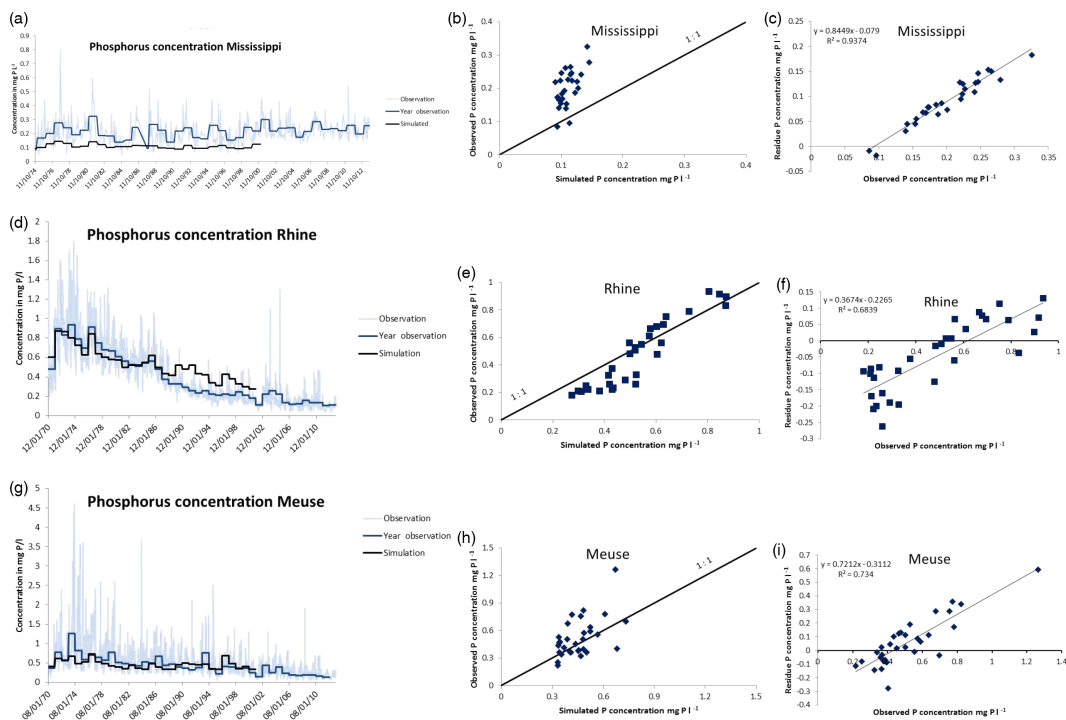


Figure 7. Comparison of modeled (black line) and measured (light blue, and aggregated yearly discharge-weighted concentrations of total P in the rivers Mississippi (a–c), Rhine (d–f) and Meuse (g–i). Panels on the left are comparisons over time; panels in the center represent plots of simulations versus observations with a 1 : 1 line, and panels on the right are the concentrations versus the residues (observation minus simulation) with a regression line.

[Title Page](#)
[Abstract](#)
[Introduction](#)
[Conclusions](#)
[References](#)
[Tables](#)
[Figures](#)

[Back](#)
[Close](#)
[Full Screen / Esc](#)
[Printer-friendly Version](#)
[Interactive Discussion](#)


Coupling global models for hydrology and nutrient loading

A. H. W. Beusen et al.

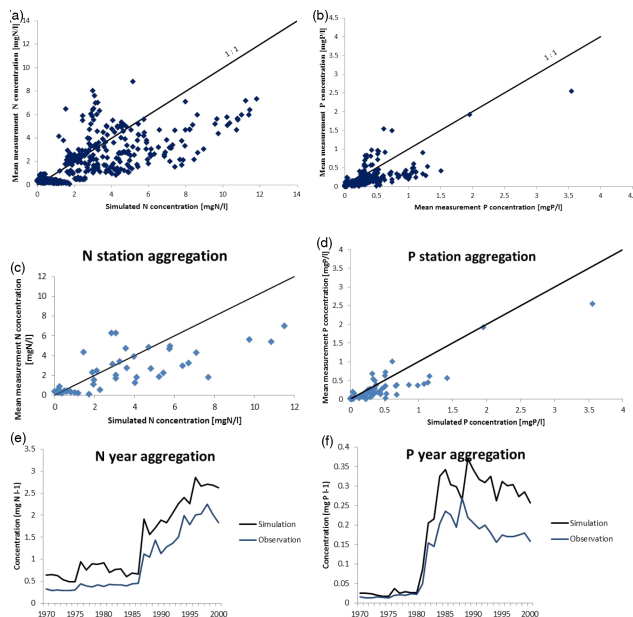


Figure 9. Comparison of simulated total N and P concentration with the EEA dataset for the period 1970–2000. **(a)** N concentration for all stations, rivers and years; **(b)** P concentration for all stations, rivers and years; **(c)** mean N concentration of all years per station; **(d)** mean P concentration of all years per station; **(e)** mean N concentration of all rivers per year; **(f)** mean P concentration of all rivers per year. Please note that the European coverage is not constant and the trend is not representative of European rivers, because the number and location of stations has changed in time, causing changes in the trend. The 1 : 1 lines are also shown in **(a)–(d)**. Comparison of modelled and observed concentrations for all individual EEA stations is in the Supplement.

Title Page

Abstract

Introduction

Conclusions

References

Tables

Figures



Back

Close

Full Screen / Esc

Printer-friendly Version

Interactive Discussion



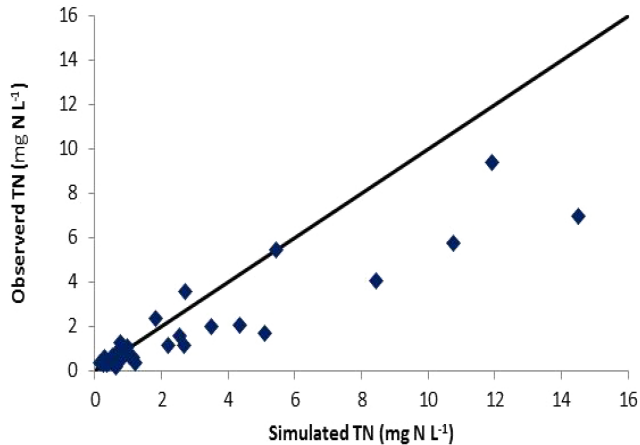


Figure 10. Comparison of simulated total N concentrations for the year 1990 with the validation dataset for the early 1990s for total N collected by Van Drecht et al. (2003) with a 1 : 1 line.

Coupling global models for hydrology and nutrient loading

A. H. W. Beusen et al.

Title Page	
Abstract	Introduction
Conclusions	References
Tables	Figures
◀	▶
◀	▶
Back	Close
Full Screen / Esc	
Printer-friendly Version	
Interactive Discussion	

